Introduction to perturbative QCD

Gudrun Heinrich[a]
[a]KIT, Karlsruhe, Germany

The aim of these lectures is to give a brief introduction to perturbative QCD; focusing on basic concepts, fixed-order calculations, and phenomenological aspects.

1 Motivation: the era of precision phenomenology

Since the spectacular completion of the Standard Model through the Higgs discovery in 2012, the Large Hadron Collider (LHC) has delivered large amounts of high quality data and will continue to do so. To date, no direct evidence for physics beyond the Standard Model has been found at the LHC; however, for new physics that resides at energy scales beyond the LHC reach, small deviations from the Standard

This chapter should be cited as: Introduction to perturbative QCD, Gudrun Heinrich, DOI: 10.23730/CYRSP-2025-009.7,
in: Proceedings of the 2023 European School of High-Energy Physics,
CERN Yellow Reports: School Proceedings, CERN-2025-009, DOI: 10.23730/CYRSP-2025-009, p.7.

Model rather than the production of new particles will be the signposts. Therefore, high precision for both, theory predictions and measurements, are the name of the game.

In perturbative quantum field theory, precision is closely related to the calculation of higher orders in an expansion in the strong coupling α_s and the electroweak coupling α. For example, a cross section can be expanded in a power series in α_s as

$$\sigma = \sigma^{\mathrm{LO}} + \alpha_s \sigma^{\mathrm{NLO}} + \alpha_s^2 \sigma^{\mathrm{NNLO}} + \dots \,, \tag{1}$$

where LO means "leading order", NLO "next-to-leading order", NNLO "next-next-to-leading order", referring to the order of the perturbative expansion in the coupling. The leading-order cross section σ^{LO} itself may contain nonzero powers of α_s or α already, while the above power series indicates the QCD corrections, which, at NLO, can be classified into *real* and *virtual* corrections. The real corrections implies the radiation of extra QCD partons (gluons or quarks), while the virtual corrections contain loops of extra virtual particles with QCD couplings. We will go through explicit examples in this lecture.

As the value of the strong coupling at the energy scale of the Z-boson mass is $\alpha_s(M_Z) \simeq 0.118$, while the electroweak (EW) coupling, $\alpha(M_Z)$, amounts to about $1/128$, QCD corrections of the same power in the coupling are in general larger than EW corrections. As a rule of thumb, the NLO QCD corrections are typically $\mathcal{O}(10\%)$, NNLO QCD corrections a few %, and NLO EW corrections also a few %. However, there are important cases where this rule does not apply, for example

- Higgs production in gluon fusion: the NLO QCD corrections are $\mathcal{O}(100\%)$, and the NNLO corrections are still in the 40% range, see Fig. 1;
- kinematic regions where EW corrections are enhanced due to large logarithms of the form $\ln\left(\frac{M_V^2}{\hat{s}}\right)$, where $\hat{s} \gg M_V^2$ and M_V is the mass of a weak boson;
- kinematic regions dominated by soft and/or collinear radiation, where large logarithms of the form $\ln\left(\frac{M^2}{p_\perp^2}\right)$ occur, for example in the transverse momentum spectrum of a particle or particle pair with invariant mass M^2 at low transverse momentum $p_\perp$. As the infrared behaviour of QED and perturbative QCD is universal, i.e. process independent, such logarithmic terms can be predicted and the perturbative series can be re-organised. This is called *resummation*;
- mixed QCD $\otimes$ EW corrections also need to be considered when percent level precision is aimed at.

At the upcoming runs of the LHC, in particular the High-Luminosity LHC, percent level statistical uncertainties will be reached for key processes. Therefore, control of the theoretical uncertainties at this level is mandatory.

2 Basics of QCD

Quantum Chromodynamics (QCD) is the theory of the strong interactions between quarks and gluons. The emergence of QCD from the quark model [38, 43, 78] started more than 50 years ago, for a review see e.g. Ref. [48]. QCD as the theory of strong interactions is nowadays well established, however it still gives us many puzzles to solve and many tasks to accomplish in order to model particle interactions in collider physics to very high accuracy.

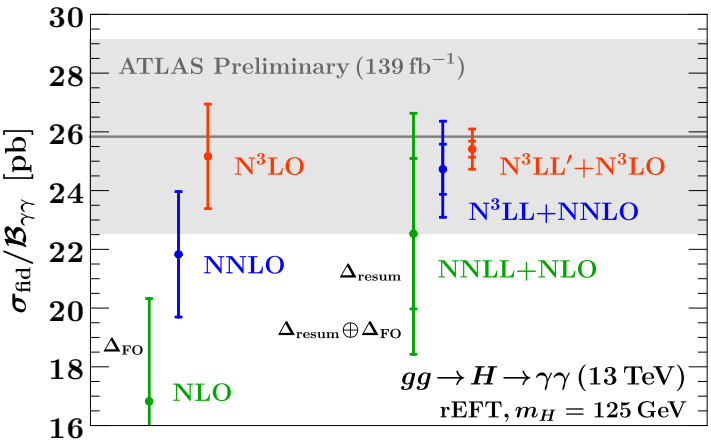

Fig. 1: Higher order QCD corrections for the fiducial cross section $gg \to H \to \gamma\gamma$, including q_T-resummation. Figure from Ref. [11].

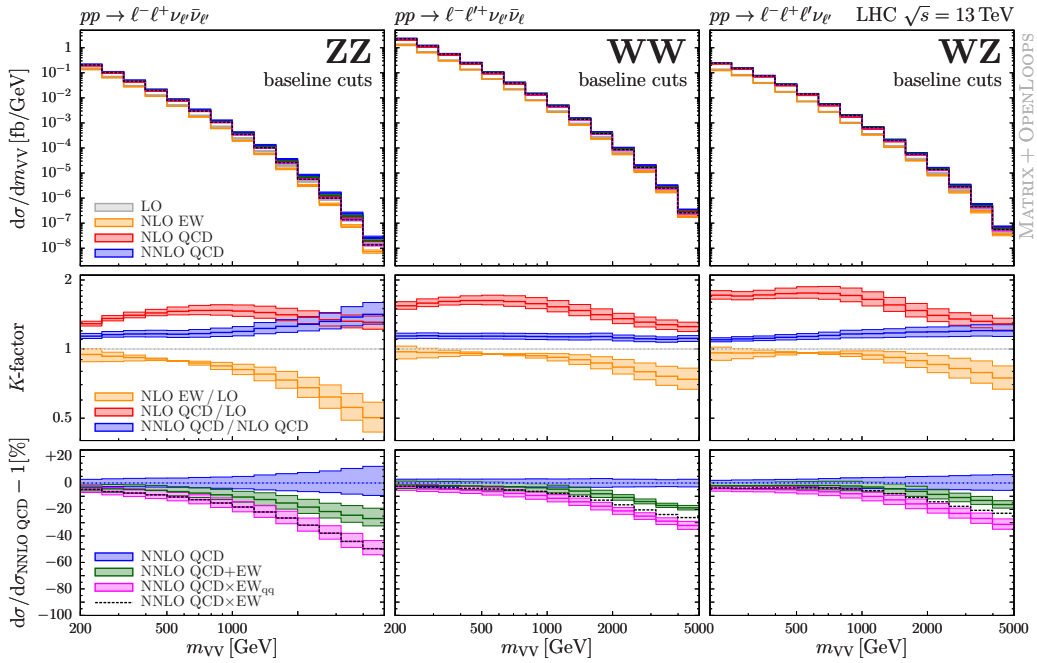

Fig. 2: Effect of electroweak corrections on vector boson pair production. Figure from Ref. [45].

The interactions are called "strong" since they are the strongest among the four fundamental forces at a length scale a bit larger than the proton radius. At a distance of 1 fm (1 fm = 10^{-15}m, the proton radius is about 0.88 fm), its strength is about 10^{38} times larger than the gravitational force. However, we will see later that the strong coupling is not constant, it varies with energy. The higher the energy at which we probe the interaction (i.e. the smaller the distance between the partons,[1] the weaker it will be. This phenomenon is called *asymptotic freedom*. At large distances between the partons, however, the interaction (coupling) becomes very strong. Therefore quarks and gluons cannot be observed as isolated particles. They are *confined* within hadrons, which are bound states of several partons.

[1]We will work in units where $\hbar = c = 1$. The mass of a proton in these units is $m_p \simeq 1\,\text{GeV} = 10^9$ eV. The conversion factor is $\hbar c \simeq 197.33$ MeV× fm.

Quarks come in six different *flavours*, denoted by u, d, c, s, t, b (up, down, charm, strange, top, bottom), grouped into three families. Hadrons can further be classified into baryons and mesons. Baryons are bound states of three quarks, for example the proton *(uud)*, mesons are quark–antiquark bound states. Pentaquarks also have been observed to exist as intermediate states.

Why "Chromodynamics"? In addition to the well-known quantum numbers like electromagnetic charge, spin or parity, quarks carry an additional quantum number called *colour*. Bound states are colour singlets. Note that without the colour quantum number, a bound state consisting e.g. of 3 u-quarks (called Δ^{++}) would violate Pauli's exclusion principle if there was no additional quantum number.

There are various approaches to make predictions and simulations based on QCD. They can be put into two broad categories: (i) perturbative QCD, which requires the coupling to be small, (ii) non-perturbative QCD, where QCD is in the strong coupling regime, such that perturbation theory is not applicable and methods such as for example "Lattice QCD" are appropriate. Our subject will be perturbative QCD.

2.1 Factorisation

A typical event at a hadron collider like the LHC is quite complicated, as sketched in Fig. 3. Since the proton is a bound state of quarks and gluons, non-perturbative aspects play a role in the initial state, and of course also in the final state, because quarks and gluons hadronize. Only the partonic cross section $\hat{\sigma}_0$ and the parton branchings can be described perturbatively. It is quite non-trivial that we can describe such complex interactions with high accuracy. The fact that we can separate the event into a part that is calculable in perturbation theory, the *hard scattering cross section*, and a non-perturbative part, is called *factorisation*. Factorisation would not be possible without *asymptotic freedom*, the fact that the strong coupling $\alpha_s(Q^2)$ decreases as the energy scale Q^2 increases.

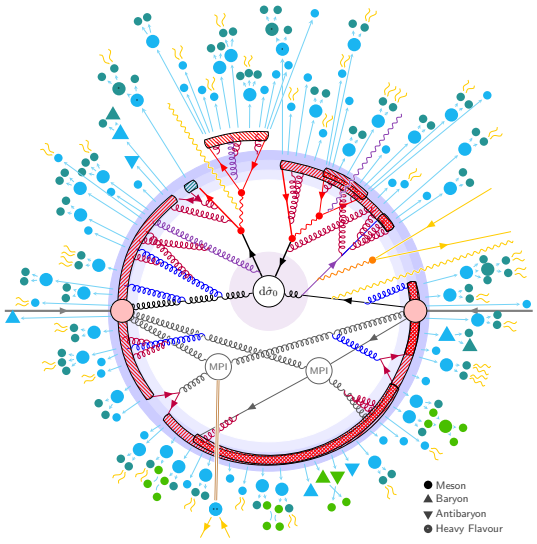

Fig. 3: Schematic picture of a LHC event. *Figure by T. Sjøstrand [48].*

The basic formula for factorisation at hadron colliders is the convolution of parton distribution functions (PDFs) with the partonic cross section.

For example, the differential cross section for a process like the production of a Higgs boson, $p_a + p_b \to H + X$, has the form

$$d\sigma_{pp\to H+X} = \sum_{i,j} \int_0^1 dx_1\, f_{i/p_a}(x_1, \alpha_s, \mu_f) \int_0^1 dx_2\, f_{j/p_b}(x_2, \alpha_s, \mu_f) \times d\hat{\sigma}_{ij}(x_1, x_2, \alpha_s(\mu_r), \mu_r, \mu_f) \; + \; \mathcal{O}\left(\frac{\Lambda}{Q}\right)^p \; . \tag{2}$$

The hard scattering cross section $d\hat{\sigma}_{ij}$ is factorised from the non-perturbative parton distribution functions f_{i/p_a}, f_{j/p_b} at the factorisation scale μ_f. Factorisation, shown schematically in Fig. 4, holds up to the so-called *power corrections* of order $\left(\frac{\Lambda}{Q}\right)^p$. The power p depends on the observable, but is always positive, and $\Lambda \simeq 250\,\text{MeV}$ is the scale where non-perturbative effects start to dominate the behaviour of the strong coupling. Therefore, the larger the typical energy scale Q^2 of the hard process, the smaller the power corrections.

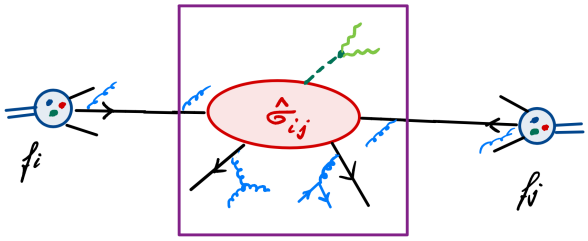

Fig. 4: Schematic picture of factorisation in hadron–hadron collisions. The purple box denotes the part that can be calculated perturbatively.

Strictly speaking, the above factorisation is called "collinear factorisation", because it assumes that the partons which are coming from the hadrons a and b have a momentum which is collinear to the parent hadron momentum. There is also the so-called "transverse momentum dependent (TMD)" factorisation, which takes into account that the partons inside the proton can have a transverse momentum relative to the beam axis. This requires transverse momentum dependent PDFs, see e.g. Ref. [70] for a review. The TMD effects can become sizeable for example in Drell-Yan production ($pp \to V \to l^+l^-$) at very low transverse momenta of the produced vector boson, or in semi-inclusive DIS (deep-inelastic scattering).

We will discuss the PDFs as well as asymptotic freedom in more detail later, here we want to stress that without factorisation, it would not be possible to produce the high precision predictions as we have them today within a strongly interacting theory, i.e. QCD.

As the PDFs themselves cannot be calculated from first principles, but need to be fitted from data, their contribution to the uncertainty budget increases in relative size the more higher orders in perturbation theory are available for the partonic cross section. The situation as of 2018 for the case of Higgs production in gluon fusion is shown in Fig. 5. While some of these uncertainties, such as $\delta(1/m_t)$, $\delta(t, b, c)$ and $\delta(EW)$, have been reduced substantially in the past few years [8, 13, 24, 25, 27], the PDF-related uncertainties are still an issue.

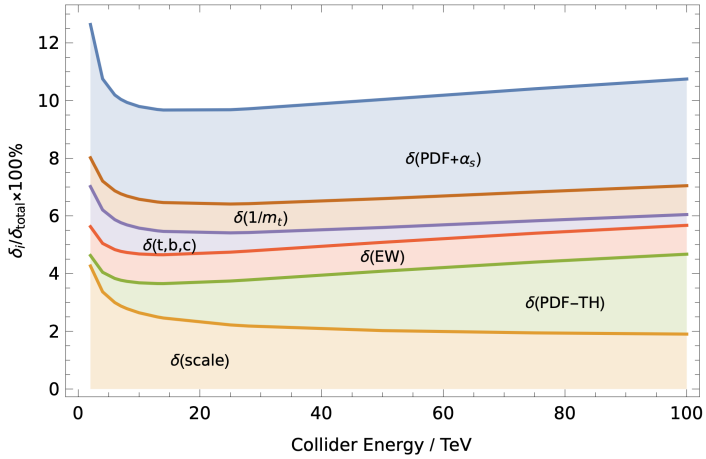

Fig. 5: Contributions to the total uncertainty for Higgs production in gluon fusion. Figure from Ref. [35].

2.2 QCD Lagrangian and Feynman rules

2.2.1 Colour algebra

The strong interactions can be described as an $SU(3)$ local gauge theory, where the "charges" are denoted as *colour*, therefore the name "Quantum Chromodynamics" (QCD). The strong interactions are embedded in the Standard Model with underlying gauge group structure $SU(3) \times SU(2)_L \times U(1)_Y$. Often the number of colours in denoted generically by N_c and the colour algebra in QCD calculations is done for a generic $SU(N_c)$ gauge group. Experimental evidence suggests that in nature $N_c = 3$, but the concept is more general. Using a generic number of colours N_c has many advantages, for example it allows us to divide the amplitudes into simpler building blocks according to their colour structure.

The group $SU(N_c)$ is an example of so-called *Lie groups* (named after Sophus Lie, Norwegian mathematician, 1842-1899), which are briefly discussed below. As we will see, the non-Abelian group structure of $SU(N_c)$ implies that gluons interact with themselves (while photons do not).

Groups

A group G is a set of elements g with a multiplication law "$\circ$": $G \times G \to G$ which satisfies:

- there is a unit element e with $g \circ e = e \circ g = g$,
- for each g an inverse g^{-1} exists, with $g \circ g^{-1} = g^{-1} \circ g = e$,
- associativity: $g_1 \circ (g_2 \circ g_3) = (g_1 \circ g_2) \circ g_3$.

For *Abelian* groups, in addition comutativity, $g_1 \circ g_2 = g_2 \circ g_1$, holds (named after Niels Henrik Abel, Norwegian mathematician, 1802-1829).

We will deal with compact Lie groups, which are groups whose elements depend analytically on a finite number of continuous parameters. The group $SU(N)$ is a Lie group whose representations U are unitary matrices with determinant one, $UU^\dagger = 1 \wedge \det U = 1$.
Other examples of Lie groups are the orthogonal groups $SO(N)$, e.g. the rotation group $SO(3)$, the symplectic groups $Sp(N)$ or the special groups G_2, F_4, E_6, E_7, E_8.

Representations

A *representation* of a group is a mapping of the group elements onto matrices, where the group multiplication laws translate to matrix multiplication (preserving the group multiplication laws), i.e. linear algebra can be used.

For Lie groups, any group element can be obtained from the identity by continuous changes in the parameters, i.e. it can be written as

$$U = \exp\{i\,\theta_a T^a\}\ ,\ \theta_a \in \mathbb{R}\ . \tag{3}$$

From $UU^\dagger = 1$ it follows that $T^a = (T^a)^\dagger$ (hermitian), from $\det U = 1$ we derive $\mathrm{Tr}(T^a) = 0$ (using $\det U = e^{\mathrm{Tr}(\ln U)}$). The set of all linear combinations $T^a\theta^a$ is a vector space and the T^a form a basis in that space. Therefore they are also called the *generators* of the group.
For the generators T^a, the commutation relation

$$[T^a,\, T^b] = i\, f^{abc}\, T^c \tag{4}$$

holds, independent of the representation, defining an algebra associated with the group. The f^{abc} are called *structure constants*. For Abelian groups the structure constants are zero.

Further, the generators satisfy the *Jacobi identity*

$$[T^a, [T^b,\, T^c]] + [T^b, [T^c,\, T^a]] + [T^c, [T^a,\, T^b]] = 0\ , \tag{5}$$

wich translates into a relation between structure constants. The generators are normalised such that

$$\mathrm{Trace}(T^a T^b) = T_R\,\delta^{ab}\ . \tag{6}$$

Usually one chooses $T_R = 1/2$ for the fundamental representation, $R = F$, which we will also do. While the (totally antisymmetric) structure constants are given in terms of generators by

$$f^{abc} = -2i\,\mathrm{Trace}\Big(T^a\big[T^b, T^c\big]\Big)\ , \tag{7}$$

we can also define totally symmetric constants by

$$d^{abc} = 2\,\mathrm{Trace}\Big(T^a\big\{T^b, T^c\big\}\Big)\ . \tag{8}$$

For QCD, two representations of $SU(N)$ will be important:
1. the *fundamental representation*: the generators are $N \times N$ matrices,
2. the *adjoint representation*: the generators of this representation are $(N^2-1)\times(N^2-1)$-matrices, i.e. the indices run over the same range as the number of generators. The number of generators is called the *dimension* of the group. So in the adjoint representation, the dimension of the vector space in which the representation matrices act equals the dimension of the group. Therefore the generators in the adjoint

representation can be expressed in terms of structure constants:

$$T^a_{bc} \underset{\text{adj}}{=} (F^a)_{bc} =: -i\, f^{abc}\ ,\ a,b,c = 1 \ldots N^2 - 1\ . \tag{9}$$

The generators of $SU(3)$ in the fundamental representation are usually defined as $t^a_{ij} = \lambda^a_{ij}/2$, where the λ^a_{ij} are also called *Gell–Mann* matrices. They are traceless and hermitian and can be considered as the $SU(3)$ analogues of the Pauli matrices for $SU(2)$.

$$\lambda^1 = \begin{pmatrix} 0 & 1 & 0 \\ 1 & 0 & 0 \\ 0 & 0 & 0 \end{pmatrix}\ ,\ \lambda^2 = \begin{pmatrix} 0 & -i & 0 \\ i & 0 & 0 \\ 0 & 0 & 0 \end{pmatrix}\ ,\ \lambda^3 = \begin{pmatrix} 1 & 0 & 0 \\ 0 & -1 & 0 \\ 0 & 0 & 0 \end{pmatrix}\ ,$$

$$\lambda^4 = \begin{pmatrix} 0 & 0 & 1 \\ 0 & 0 & 0 \\ 1 & 0 & 0 \end{pmatrix}\ ,\lambda^5 = \begin{pmatrix} 0 & 0 & -i \\ 0 & 0 & 0 \\ i & 0 & 0 \end{pmatrix}\ ,\ \lambda^6 = \begin{pmatrix} 0 & 0 & 0 \\ 0 & 0 & 1 \\ 0 & 1 & 0 \end{pmatrix}\ ,$$

$$\lambda^7 = \begin{pmatrix} 0 & 0 & 0 \\ 0 & 0 & -i \\ 0 & i & 0 \end{pmatrix}\ ,\ \lambda^8 = \frac{1}{\sqrt{3}} \begin{pmatrix} 1 & 0 & 0 \\ 0 & 1 & 0 \\ 0 & 0 & -2 \end{pmatrix}\ .$$

Colour in QCD

Quark fields transform according to the fundamental representation of $SU(3)$. Therefore the Feynman rules for the quark–gluon vertex involve t^a_{ij} where $i,j = 1 \ldots N_c$ run over the colours of the quarks (the *degree* of the group), while $a = 1 \ldots N_c^2 - 1$ runs over the dimension of the group. Gluons transform according to the adjoint representation of $SU(3)$. Therefore the Feynman rule for the three-gluon vertex contains $(F^a)_{bc} = -i\, f^{abc}$.

The gluons can be regarded as a combination of coloured lines, as depicted in Fig. 6, or, more precisely, as a combination of colours and anticolours. Contracting colour indices is graphically equivalent

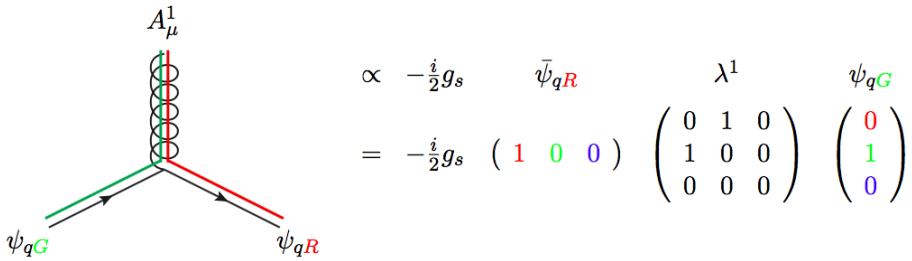

Fig. 6: Representation of the gluon as a double colour line. *Picture from Ref. [72].*

to connecting the respective colour (or anticolour) lines. The representation of the quark–gluon vertex in Fig. 6 embodies colour conservation, whereby the colour–anticolour quantum numbers carried by the $q\bar{q}$ pair are transferred to the gluon. The eight gluons can be regarded as all possible colour–anticolour

combinations, where the combination corresponding to λ^8 would be $\frac{1}{\sqrt{6}}(r\bar{r} + g\bar{g} - 2b\bar{b})$ (with r: red, g: green, b: blue). Note that the singlet combination $\frac{1}{\sqrt{3}}(r\bar{r} + g\bar{g} + b\bar{b})$ does not occur for the gluon because the singlet cannot mediate colour.

Casimir operators

The sums $\sum_{a,j} t^a_{ij} t^a_{jk}$ and $\sum_{a,d} F^a_{bd} F^a_{dc}$ have two free indices in the fundamental and adjoint representation, respectively. One can show that these sums are invariant under $SU(N_c)$ transformations, and therefore must be proportional to the unit matrix:

$$\sum_{j,a} t^a_{ij} t^a_{jk} = C_F\, \delta_{ik}\,, \qquad \sum_{a,d} F^a_{bd} F^a_{dc} = C_A\, \delta_{bc}\,. \tag{10}$$

The constants C_F and C_A are the eigenvalues of the quadratic *Casimir operator* in the fundamental and adjoint representation, respectively. Casimir operators commute with every element of the group. The Casimir eigenvalues can be expressed in terms of the number of colours N_c as

$$C_F = T_R \frac{N_c^2 - 1}{N_c}\,,\; C_A = 2\, T_R\, N_c\,. \tag{11}$$

Graphical representation of the colour algebra

The commutation relation (4) in the fundamental representation can be represented graphically by[2]

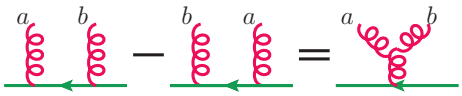

$$t^a t^b - t^b t^a = i\, f^{abc}\, t^c$$

Multiplying this commutator first with another colour charge operator, summing over the fermion index and then taking the trace over the fermion line (i.e. multiplying with δ_{ik}) we obtain the representation of the three-gluon vertex as traces of products of colour charges:

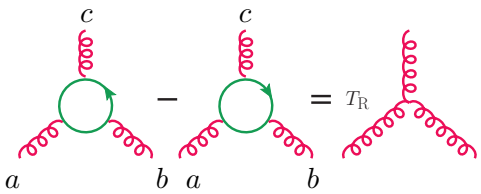

$$\mathrm{Trace}(t^a t^b t^c) - \mathrm{Trace}(t^c t^b t^a) = i\; T_R f^{abc} \tag{12}$$

Such relations allow us to compute the colour algebra structure of a QCD diagram, independent of the kinematics. For example, taking the trace of the identity (δ_{ij} resp. δ_{ab}) in the fundamental resp. in the adjoint representation we obtain

[2] Some of the figures have been taken from Ref. [75].

respectively. Then, using the expressions for the fermion and gluon propagator insertions, we find

There is also a very useful identity for the product of two colour matrices in the fundamental representation, occurring when a gluon is exchanged between two quark lines, and following from representing the gluon as a double quark line,

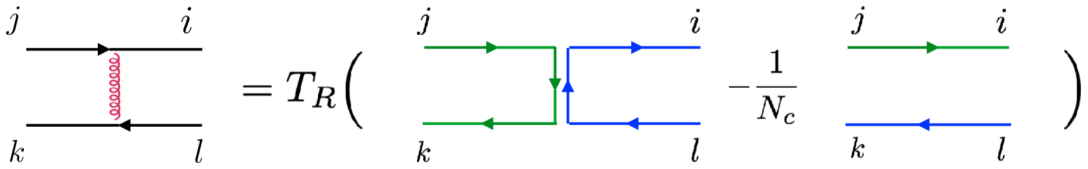

corresponding to

$$t^a_{ij} t^a_{kl} = T_R \left(\delta_{il}\delta_{kj} - \frac{1}{N_c}\delta_{ij}\delta_{kl} \right) \,. \tag{13}$$

The second term $\sim 1/N_c$ implements the condition that the generators are traceless, and the picture indicates that a gluon which mediates between quarks of the same colour does not exist, because it would be a colour singlet.

Colour decomposition

From the representation of gluons as double colour lines it follows that any tree-level diagram for n-gluon scattering can be expressed in terms of traces over generators t^a_{ij}, as depicted in Fig. 7. This observation leads to the so-called *colour decomposition* of amplitudes, which allows to separate the colour information from the kinematic part of an amplitude. An amplitude for n-gluon scattering can be

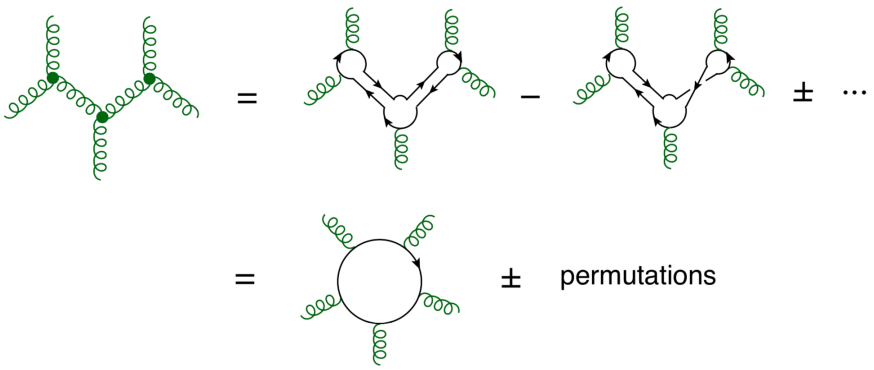

Fig. 7: Colour decomposition of tree-level gluon amplitudes. *Figure from Ref. [31].*

written as

$$\mathcal{A}_n^{\text{tree}}\left(\{k_i,\lambda_i,a_i\}\right) = g_s^{n-2} \sum_{\sigma\in S_n/Z_n} \text{Trace}\left(t^{a_{\sigma(1)}}\cdots t^{a_{\sigma(n)}}\right) A_n^{\text{tree}}(\sigma(1^{\lambda_1}),\ldots,\sigma(n^{\lambda_n}))\,, \tag{14}$$

where k_i, λ_i are the gluon momenta and helicities, a_i the colour indices and $A_n^{\text{tree}}(1^{\lambda_1},\ldots,n^{\lambda_n})$ are the *partial amplitudes*, which contain all the kinematic information. S_n is the set of all permutations of n objects, while Z_n is the subset of cyclic permutations, which preserves the trace; the latter are excluded in the sum over the set S_n/Z_n.

The advantage of this representation is that the partial amplitudes A_n^{tree} are simpler to calculate than the full amplitude because they are *colour ordered*: they only receive contributions from diagrams with a particular cyclic ordering of the gluons. This implies that for the partial amplitudes, the infrared singularities related to external massless particles becoming collinear can only occur in a subset of momentum channels, those with cyclically adjacent momenta. For example, the five-point partial amplitudes $A_5^{\text{tree}}(1^{\lambda_1},2^{\lambda_2},3^{\lambda_3},4^{\lambda_4},5^{\lambda_5})$ can only have poles in s_{12}, s_{23}, s_{34}, s_{45}, s_{51}, and not in s_{13}, s_{24}, s_{35}, s_{41} or s_{52}, where $s_{ij} \equiv (k_i+k_j)^2$.

The colour decomposition is not limited to gluons only, it also can be applied when quarks are involved. For example, a tree amplitude with a $q\bar{q}$ pair and otherwise gluons can be written as

$$\mathcal{A}_n^{\text{tree}} = g_s^{n-2} \sum_{\sigma\in S_{n-2}} \left(t^{a_{\sigma(3)}}\cdots t^{a_{\sigma(n)}}\right)_{j_1 i_2} A_n^{\text{tree}}(1_{\bar{q}}^{\lambda_1},2_q^{\lambda_2},\sigma(3^{\lambda_3}),\ldots,\sigma(n^{\lambda_n}))\,. \tag{15}$$

Using eq. (13), there is yet another possibility to perform the colour decomposition, based on Kronecker δ_{ij}'s only, also called *colour flow decomposition* [62]. The computational gain when using colour decomposition to calculate amplitudes with n gluons is illustrated in Table 1. At loop level, colour

	# diagrams	
n	partial amplitude	full amplitude
4	3	4
5	10	25
6	36	220
7	133	2485
8	501	34300
9	1991	559405
10	7335	10525900
11	28199	224449225
12	108281	5348843500

Table 1: Number of diagrams for tree-level n-gluon amplitudes. *Table from Ref. [62].*

decomposition can also be performed [9, 29, 31, 53, 65, 68].

Another advantage of colour decomposition is the possibility to approximate complex calculations by the leading-colour approximation, where only the leading term in N_c is retained. A detailed study of subleading colour effects in single jet inclusive and dijet production at NNLO can be found in Ref. [20].

2.2.2 *Experimental evidence for the existence of colour*

The colour factors C_F and C_A can be measured indirectly from jet production cross sections. Jets can

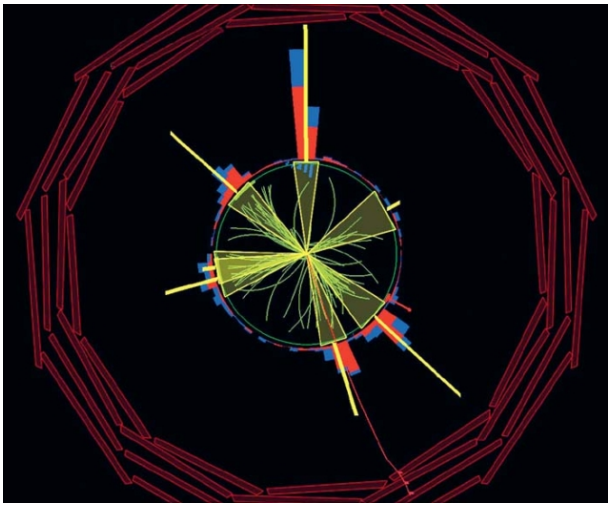

Fig. 8: Example of a 6-jet event measured by CMS. *Source: CERN Courier.*

be pictured as clusters of particles (usually hadrons) which are close to each other in phase space, resp. in the detector, see Fig. 8, showing a 6-jet event measured by CMS. Jets will be discussed in more detail in Section 4.

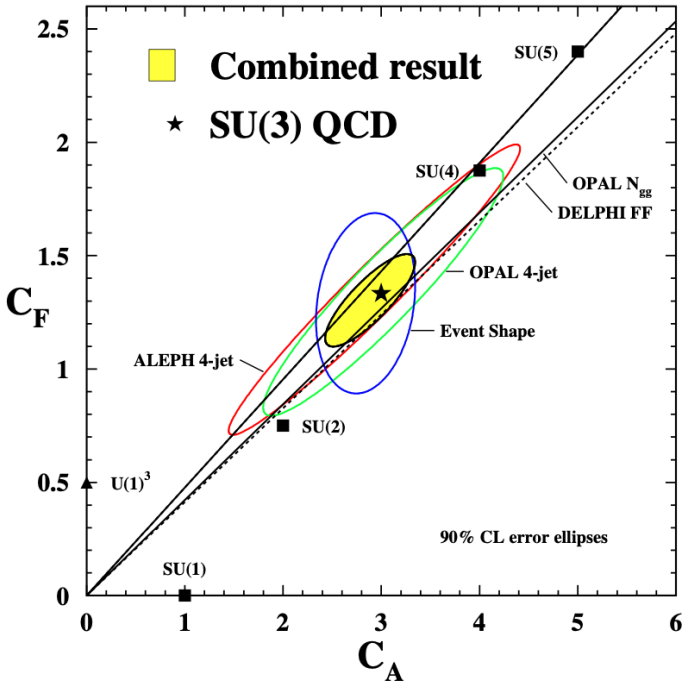

Fig. 9: Evidence for colour-$SU(3)$ from jet measurements at the LEP collider. Figure from Ref. [56].

The theory predictions for the jet cross sections depend on the number of colours, as can be seen in Fig. 9 for a measurement of jet cross sections at LEP. The leading-colour contribution to the squared

n-gluon matrix elements relevant at hadron colliders, summed over colours (and helicities), is given by

$$|\mathcal{M}_n|^2 = \left(g^2 N_c\right)^{n-2} \left(N_c^2 - 1\right) \sum_{\sigma \in S_n/Z_n} \left\{ |\mathcal{A}_n(\sigma(1), \cdots, \sigma(n))|^2 + \mathcal{O}\left(\frac{1}{N_c^2}\right) \right\} ,$$

so if N_c was different, the jet cross sections would change drastically. How well they agree with recent measurements is shown in Fig. 10.

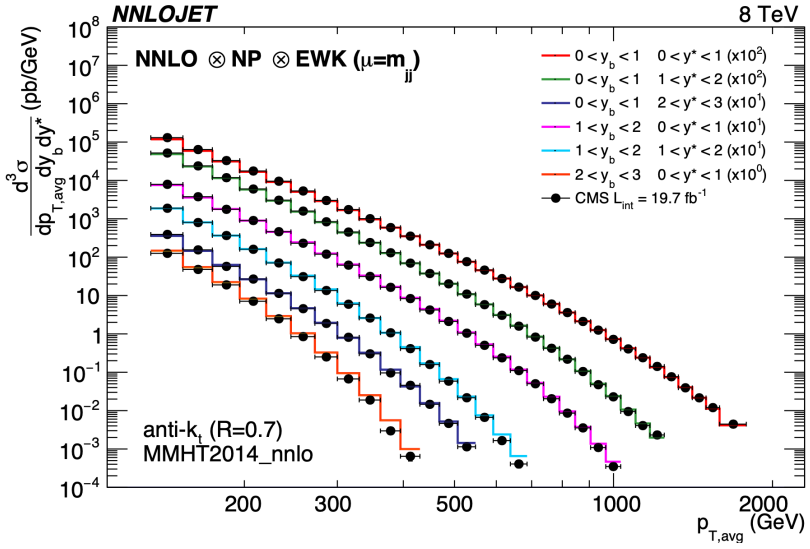

Fig. 10: Triple-differential two-jet cross sections at NNLO compared to CMS data. Figure from Ref. [42].

A good theoretical description of jets at the LHC is important for many reasons. For example, jet data are very important to constrain the PDFs and jet cross sections are used for precision determinations of the strong coupling α_s. Furthermore, for jets originating from massless partons, there is energy available to go up to very high values in the jet p_T spectrum, $\mathcal{O}$(2–4 TeV), which is a kinematic region sensitive to new physics. Jets recoiling against missing transverse energy ("missing" in the total transverse energy budget) could be a signal for an unknown heavy particle (for example related to dark matter) decaying into something not visible in the detector.

Hadronic R-ratio

Among the historically early evidence for the existence of 3 colour quantum numbers is the so-called *hadronic R-Ratio*, the total cross section for the production of hadrons in electron–positron collisions, divided by the cross section for the production of a muon–antimuon pair, as a function of the centre-of-mass energy s,

$$R(s) = \frac{\sigma(e^+e^- \to \text{ hadrons})}{\sigma(e^+e^- \to \mu^+\mu^-)} . \tag{16}$$

Hadrons are bound states of quarks and gluons, so for the numerator, at microscopic level, this means that a fermion–antifermion pair $f\bar{f}$ is created as soon as the centre-of-mass energy s is sufficient to produce two quarks of mass m_f . The interaction proceeds via the exchange of a virtual photon, see

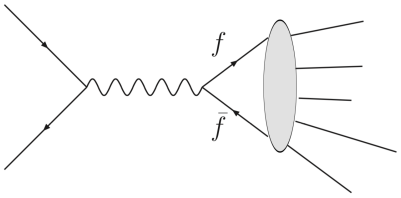

Fig. 11: The production of hadrons in e^+e^- collisions via virtual photon exchange.

Fig. 11 (neglecting Z-boson exchange). The electromagnetic interaction (the photon) only sees the electromagnetic charge e_f of the fermions, be it quarks or leptons. Therefore one would expect that at large energies

$$R(s) = \frac{\sum_{f=u,d,s,c,\ldots} \sigma(e^+e^- \to f\bar{f})}{\sigma(e^+e^- \to \mu^+\mu^-)} \overset{s\,\text{large}}{\longrightarrow} \sum_{f=u,d,s,c,\ldots} e_f^2\, \theta(s - 4m_f^2)\ . \tag{17}$$

However this is not what has been found experimentally. The experimental results agree with the expression

$$R(s) = N_c \sum_{f=u,d,s,c,\ldots} e_f^2\, \theta(s - 4m_f^2)\ , \tag{18}$$

with $N_c = 3$. Above the bottom quark pair production threshold, we have ($m_b \simeq 4.2$ GeV)

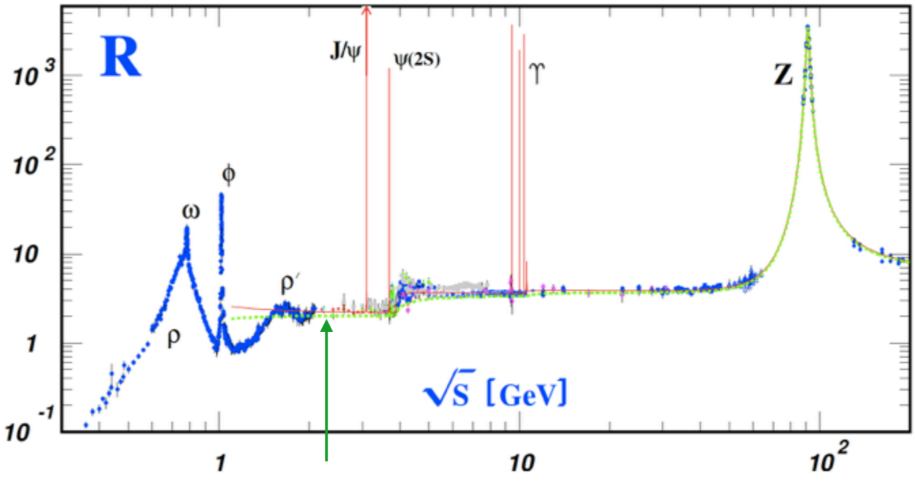

Fig. 12: R-Ratio vs. center-of-mass energy. *Figure from Ref. [57].*

$$R(s) = N_c \sum_{f=u,d,s,c,b} e_f^2\, \theta(s - 4m_f^2) = 3\left(\tfrac{4}{9} + \tfrac{1}{9} + \tfrac{1}{9} + \tfrac{4}{9} + \tfrac{1}{9}\right) = \tfrac{11}{3}\ . \tag{19}$$

The stepwise increase of the R-ratio can be seen in Fig. 12, even though it is blurred by the resonances ρ, ω, ϕ, etc. In Fig. 13 the quark pair production thresholds without the resonances are shown. The top quark does not show up here, it is heavier than the Z-boson, $m_t \simeq 173$ GeV, and it decays before it hadronises.

Another example which is often given as an argument for $N_c = 3$ is the decay rate of a neutral

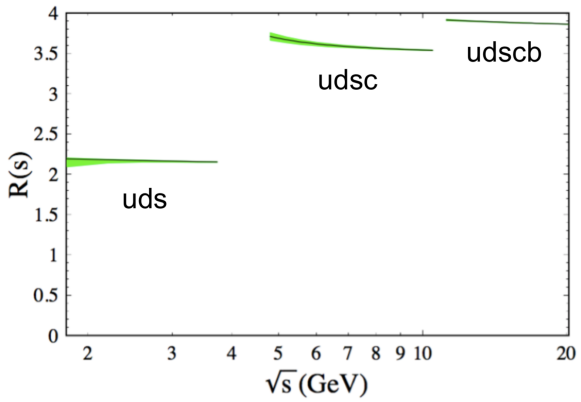

Fig. 13: R-ratio without resonance effects. *Figure from Ref. [50].*

.

pion into two photons:

$$\Gamma(\pi^0 \to \gamma\gamma) \simeq \alpha^2 \frac{m_\pi^3}{f_\pi^2}(e_u^2 - e_d^2)^2 N_c^2 \ . \tag{20}$$

However, there could be cancellations between N_c and a different denominator in the fractional charges of the quarks: for $e_u = (1/N_c + 1)/2$, $e_d = (1/N_c - 1)/2$ the decay rate would be independent of N_c (and a relation between N_c and the fractional charges of the quarks also makes sense in view of anomaly cancellation). Therefore, Eq. (20) alone cannot be seen as a full proof of N_c being equal to 3.

A more theoretical argument for the existence of a colour quantum number has been mentioned already: it is given by the fact that bound states consisting of three quarks, e.g. the delta-resonance Δ^{++} consisting of 3 u-quarks, would violate Pauli's exclusion principle if there was no additional quantum number (which implies that this state must be totally antisymmetric in the colour indices).

2.2.3 QCD Lagrangian

An important concept in QCD (and in quantum field theories in general) is the formulation as a *local* gauge theory. This means that the gauge transformation parameter depends itself on x, the position in space–time.

Fermionic part of the QCD Lagrangian

Consider the quark fields $q_f^j(x)$ for just one quark flavour f. The index j labels the colour, $j = 1, \ldots, N_c$. Treating the quarks as free Dirac fields, we have

$$\mathcal{L}_q^{(0)}(q_f,\, m_f) = \sum_{j,k=1}^{N_c} \bar{q}_f^j(x)\ (i\,\gamma_\mu \partial^\mu - m_f)\delta_{jk}\ q_f^k(x)\ , \tag{21}$$

where the Dirac-matrices γ_μ satisfy the anti-commutation relation (Clifford algebra)

$$\{\gamma^\mu, \gamma^\nu\} \ = \ 2\, g^{\mu\nu}\ . \tag{22}$$

Now let us apply a group transformation (i.e. a "rotation" in colour space) on the fermion fields. It has the form

$$q_k \to q'_k = U_{kl}\, q^l \ , \quad \bar{q}_k \to \bar{q}'_k = \bar{q}^l U^{-1}_{lk} \ , \tag{23}$$

with

$$U_{kl} = \exp\left\{ i \sum_{a=1}^{N_c^2-1} t^a\, \theta^a \right\}_{kl} \equiv \exp\left\{ i\, \boldsymbol{t} \cdot \boldsymbol{\theta} \right\}_{kl} \ , \tag{24}$$

where θ^a are the group transformation parameters and $(t^a)_{kl}$ the generators of $SU(N_c)$ in the fundamental representation. The Lagrangian of free Dirac fields remains invariant under this transformation as long as it is a *global* transformation, i.e. as long as the θ^a do not depend on x: $\mathcal{L}_q^{(0)}(q) = \mathcal{L}_q^{(0)}(q')$.

However, we aim at *local* gauge transformations, where the gauge transformation parameter θ in Eq. (24) depends on x. In QED, where the underlying gauge group is $U(1)$, a global transformation would just be a phase change. The requirement of a free electron field to be invariant under *local* transformations $\theta = \theta(x)$ leads to the introduction of a *gauge field* A_μ, the photon. The analogous is true for QCD: requiring local gauge invariance under $SU(N_c)$ leads to the introduction of gluon fields A^a_μ to arrive at a gauge invariant Lagrangian, wich can be seen as follows:
As the local gauge transformation

$$U(x) = \exp\left\{ i\, \boldsymbol{t} \cdot \boldsymbol{\theta}(\boldsymbol{x}) \right\} \tag{25}$$

depends on x, the derivative of the transformed quark field $q'(x)$ reads

$$\partial_\mu\, q'(x) = \partial_\mu \left(U(x) q(x) \right) = U(x) \partial_\mu\, q(x) + \left(\partial_\mu U(x) \right)\, q(x) \ . \tag{26}$$

To keep $\mathcal{L}_q$ gauge invariant, we can remedy the situation caused by the second term above by introducing the coupling to a gauge field which transforms accordingly. We define a *covariant derivative* D^μ, depending on A^μ_a, by

$$\left(D^\mu[A] \right)_{ij} = \delta_{ij} \partial^\mu + i\, g_s\, t^a_{ij} A^\mu_a \ , \tag{27}$$

or, without index notation

$$\boldsymbol{D}^\mu[\boldsymbol{A}] = \partial^\mu + i\, g_s\, \boldsymbol{A}^\mu \ , \tag{28}$$

where $\boldsymbol{A}^\mu = t^a\, A^\mu_a$ (sum over $a = 1 \ldots N_c^2 - 1$ understood). The fields A^μ_a are the *gluons*. The Lagrangian corresponding to this "minimal coupling" of a gluon field reads

$$\mathcal{L}_q(q_f,\, m_f) = \sum_{j,k=1}^{N_c} \bar{q}^j_f(x)\, \left(i\, \gamma_\mu \boldsymbol{D}^\mu[\boldsymbol{A}] - m_f \right)_{jk}\, q^k_f(x) \ . \tag{29}$$

To keep this Lagrangian invariant under local gauge transformations, we therefore must have

$$\begin{aligned} \boldsymbol{D}^\mu[\boldsymbol{A}'] q'(x) &\stackrel{!}{=} U \Big(\boldsymbol{D}^\mu[\boldsymbol{A}]\, q(x) \Big) \\ \Rightarrow \partial_\mu + i g_s \boldsymbol{A}'_\mu &\stackrel{!}{=} U \left(\partial_\mu + i g_s \boldsymbol{A}_\mu \right) U^{-1} \end{aligned} \tag{30}$$

Eq. (30) gives a condition on $\boldsymbol{A}'_\mu(x)$, which can be derived using $U\,\partial_\mu U^{-1} = -(\partial_\mu U)U^{-1} + \partial_\mu(UU^{-1})$. Therefore the gluon fields need to transform under general $SU(N_c)$ transformations as

$$\boldsymbol{A}'_\mu = U(x)\boldsymbol{A}_\mu U^{-1}(x) + \frac{i}{g_s}(\partial_\mu U(x))U^{-1}(x)\ . \tag{31}$$

Purely gluonic part of the QCD Lagrangian

The purely gluonic part of the QCD Lagrangian can be described by the so-called Yang–Mills Lagrangian (C. N. Yang, R. Mills, 1954)

$$\mathcal{L}_{\rm YM} = -\frac{1}{4}F^a_{\mu\nu}\,F^{a,\mu\nu}\ , \tag{32}$$

where the non-Abelian field strength tensor $F^a_{\mu\nu}$ is given by

$$F^a_{\mu\nu} = \partial_\mu A^a_\nu - \partial_\nu A^a_\mu - g_s\,f^{abc}A^b_\mu A^c_\nu\ . \tag{33}$$

We can also express everything in terms of $\boldsymbol{A}^\mu = t^a\,A^\mu_a$ and write the field strength tensor as

$$\boldsymbol{F}_{\mu\nu}(x) = \sum_{a=1}^{N_c^2-1} F^a_{\mu\nu}(x)\,t^a = \frac{i}{g_s}\,[\,\boldsymbol{D}_\mu, \boldsymbol{D}_\nu\,]\ , \tag{34}$$

which implies

$$\mathcal{L}_{\rm YM} = -\frac{1}{4}\,F^a_{\mu\nu}\,F^{a,\mu\nu} = -\frac{1}{2}\,{\rm Trace}\,[\boldsymbol{F}_{\mu\nu}\boldsymbol{F}^{\mu\nu}]\ . \tag{35}$$

Note that the term proportional to f^{abc} in the expression for $F^a_{\mu\nu}$, which reflects the non-Abelian structure and is not present in QED, leads to terms with 3 or 4 gluon fields in the Lagrangian and therefore to self-interactions between the gluons.

Finally, we obtain for the "classical" QCD Lagrangian

$$\mathcal{L}_c = \mathcal{L}_{\rm YM} + \mathcal{L}_q = -\frac{1}{4}F^a_{\mu\nu}\,F^{a,\mu\nu} + \sum_{j,k=1}^{N_c}\bar{q}^j_f(x)\,(i\,\gamma_\mu D^\mu[A] - m_f)_{jk}\,q^k_f(x)\ . \tag{36}$$

Gauge fixing

We are not quite there yet with the complete QCD Lagrangian. The "classical" QCD Lagrangian $\mathcal{L}_c$ contains degenerate field configurations (i.e. they are equivalent up to gauge transformations). This leads to the fact that the bilinear operator in the gluon fields is not invertible, such that it is not possible to construct a propagator for the gluon fields. The propagator is usually derived from the bilinear term in the fields in the path integral for free fields, with the generating functional (introducing the d'Alembert operator $\Box \equiv \partial_\mu\partial^\mu$)

$$Z_0[J] = \int \mathcal{D}A_\mu(x)\,e^{i\int d^4x\left[\frac{1}{2}A^a_\mu(x)(g^{\mu\nu}\Box - \partial^\mu\partial^\nu)A^b_\nu(x)\delta_{ab} + J^a_\mu A^\mu_a\right]}\ . \tag{37}$$

In momentum space this leads to the following condition for the propagator $\Delta_{\mu\nu}(p)$, where we suppress colour indices as the propagator is diagonal in colour space, i.e. we leave out overall factors δ^{ab},

$$i\,\Delta_{\mu\rho}(p)\,\left[p^2 g^{\rho\,\nu}\,-\,p^\rho p^\nu\right] = g_\mu^\nu\,. \tag{38}$$

However, we also have

$$\left[p^2 g^{\rho\,\nu} - p^\rho p^\nu\right] p_\nu = 0\,, \tag{39}$$

which means that the matrix $\left[p^2 g^{\rho\,\nu}\,-\,p^\rho p^\nu\right]$ is not invertible because it has at least one eigenvalue equal to zero. We have to remove the physically equivalent configurations from the classical Lagrangian. This is called *gauge fixing*. We can achieve this by imposing a constraint on the fields A_μ^a, adding a term to the Lagrangian with a Lagrange multiplier.

For example, *covariant gauges* are defined by the requirement $\partial_\mu A^\mu\,(x) = 0$ for any x. Adding

$$\mathcal{L}_{\rm GF} = -\frac{1}{2\lambda}\,(\partial_\mu A^\mu)^2\,, \qquad \lambda\,\in\,\mathbb{R},$$

to $\mathcal{L}$, the bilinear term has the form

$$i\,\left(p^2 g^{\mu\nu} - \left(1 - \frac{1}{\lambda}\right) p^\mu p^\nu\right),$$

with inverse

$$\Delta_{\mu\nu}(p) = \frac{-i}{p^2 + i\,\varepsilon}\left[g_{\mu\nu} - (1-\lambda)\frac{p_\mu p_\nu}{p^2}\right]\,. \tag{40}$$

The so-called $i\,\varepsilon$–prescription ($\varepsilon\,>\,0$) shifts the poles of the propagator slightly off the real p^0-axis (where p^0 is the energy component) and ensures the correct causal behaviour of the propagators. Choosing $\lambda = 1$ is called *Feynman gauge*, and $\lambda = 0$ is called *Landau gauge*. Of course, physical results must be independent of λ.

In covariant gauges, unphysical degrees of freedom (longitudinal and time-like polarisations) also propagate. The effect of these unwanted degrees of freedom is cancelled by the ghost fields, which are coloured complex scalars obeying Fermi statistics. Unphysical degrees of freedom and the ghost fields can be avoided by choosing *axial gauges* (also called *physical gauges*). The axial gauge is defined by introducing an arbitrary vector n^μ with $p\cdot n \neq 0$, to impose the constraint

$$\mathcal{L}_{\rm GF} = -\frac{1}{2\alpha}\,(n^\mu A_\mu)^2\,, \tag{41}$$

which leads to

$$\Delta_{\mu\nu}(p,n) = \frac{-i}{p^2 + i\,\varepsilon}\left(g_{\mu\nu} - \frac{p_\mu n_\nu + n_\mu p_\nu}{p\cdot n} + \frac{n^2\,p_\mu p_\nu}{(p\cdot n)^2}\right). \tag{42}$$

The so-called *light-cone gauge* is characterised by $n^2 = 0$. Note that the axial gauge propagator (42) satisfies

$$\Delta_{\mu\nu}\,(p,n)\;p^\mu = 0\,, \quad \Delta_{\mu\nu}\,(p,n)\;n^\mu = 0\,.$$

Thus, only 2 degrees of freedom propagate (transverse ones in the $n^\mu + p^\mu$ rest frame). The price to pay

by choosing an axial gauge instead of a covariant one is that the propagator looks more complicated and that it diverges when p^μ becomes parallel to n^μ. In the light-cone gauge we have

$$\begin{aligned}\Delta_{\mu\nu}(p,n) &= \frac{i}{p^2 + i\,\varepsilon}\, d_{\mu\nu}(p,n)\ , \\ d_{\mu\nu}(p,n) &= -g_{\mu\nu} + \frac{p_\mu n_\nu + n_\mu p_\nu}{p\cdot n} = \sum_{\lambda=1,2} \epsilon^\lambda_\mu(p) \left(\epsilon^\lambda_\nu(p)\right)^*\ ,\end{aligned} \tag{43}$$

where $\epsilon^\lambda_\mu(p)$ is the polarisation vector of the gluon field with momentum p and polarisation λ. This means that only the two physical polarisations ($\lambda = 1, 2$) propagate. In contrast, in Feynman gauge, we have

$$d_{\mu\nu}(p) = -g_{\mu\nu} = \sum_{\lambda=0}^{3} \epsilon^\lambda_\mu(p) \left(\epsilon^\lambda_\nu(p)\right)^*\ , \tag{44}$$

where the polarisation sum also runs over non-transverse gluon polarisations. Unphysical polarisations that occur in loops will be cancelled by the corresponding loops involving ghost fields.

Faddeev–Popov ghost fields

The introduction of a gauge fixing constraint is achieved by inserting unity in the form

$$1 = \int \mathcal{D}\theta(x)\, \delta(G^a(A^\theta) - h^a(x))\, \det\left(\frac{\delta G^a(A^\theta)}{\delta\theta}\right) \tag{45}$$

into the generating functional $Z[J]$. A^θ denotes all fields which are equivalent through a gauge transformation involving the group parameter θ. In covariant gauges $h^a(x) = \partial^\mu A^a_\mu(x)$. The determinant $\det\left(\frac{\delta G^a(A^\theta)}{\delta\theta}\right) =: \Delta_{FP}(A)$ can be written as a functional integral over anti-commuting fields $\eta^a(x), \bar\eta^b(x)$,

$$\Delta_{FP}(A) = \int \mathcal{D}\bar\eta\mathcal{D}\eta\, e^{i\int d^4x d^4y\, \bar\eta^a(x) M_{ab}(x,y)\, \eta^b(y)} \quad \text{with} \quad M_{ab}(x,y) = \frac{\delta G^a(A^\theta(x))}{\delta\theta^b(y)}\ . \tag{46}$$

The fields $\bar\eta^a(x), \eta^b(x)$ are the so-called *Faddeev–Popov*-fields or *ghost* fields, they are complex scalar fields, which however obey Fermi-statistics, so they anti-commute. They cannot occur as external states because they do not have physical polarisations.

The additional term in the Lagrangian as a result of the procedure sketched above reads

$$\mathcal{L}_{FP} = \bar\eta_a\, M^{ab}\, \eta_b\ . \tag{47}$$

In covariant gauges, the operator M^{ab} (also called Faddeev–Popov matrix) is given by

$$M^{ab}_{\text{cov}} = \delta^{ab}\,\partial_\mu\partial^\mu + g_s\, f^{abc} A^c_\mu \partial^\mu\ . \tag{48}$$

Here we can see that in QED (or another Abelian gauge theory) the second term is absent, such that the Faddeev–Popov matrix does not depend on any field and therefore Δ_{FP} can be absorbed into the

normalisation of the path integral, such that no ghost fields are needed in Abelian gauge theories.

In axial gauges, the Faddeev–Popov matrix becomes

$$M^{ab}_{\text{axial}} = \delta^{ab}\, n_\mu \partial^\mu + g_s\, f^{abc}\, n_\mu A^\mu_c \,, \tag{49}$$

such that, due to the gauge fixing condition $n \cdot A = 0$, the matrix is again independent of the gauge field and therefore can be absorbed into the normalisation, such that no ghost fields propagate.

Collecting all contributions, we finally have derived the full QCD Lagrangian

$$\boxed{\mathcal{L}_{QCD} = \mathcal{L}_{\text{YM}} + \mathcal{L}_q + \mathcal{L}_{GF} + \mathcal{L}_{FP} \,.} \tag{50}$$

2.2.4 QCD Feynman rules

Feynman rules are something like a Lego brick box containing pieces that can be assembled to an expression describing a process such as the scattering of elementary particles or the decay of a particle. They can be derived from the interaction terms in the action, resp. the Lagrangian. There are also automated tools that can derive Feynman rules from a given Lagrangian, see e.g. [1, 26].

We will not derive the QCD Feynman rules from scratch, but just state them below.

Propagators: ($i\varepsilon$ prescription understood)

gluon propagator: $\Delta^{ab}_{\mu\nu}(p) = \delta^{ab}\, \Delta_{\mu\nu}(p)$

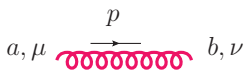

quark propagator: $\Delta^{ij}_q\,(p) = \delta^{ij}\, i\, \frac{\not{p}+m}{p^2-m^2}$

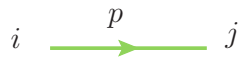

ghost propagator: $\Delta^{ab}\,(p) = \delta^{ab}\, \frac{i}{p^2}$

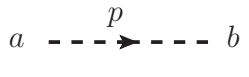

Vertices:

quark–gluon: $\Gamma^{\mu,\,a}_{gq\bar{q}} = -i\, g_s\, (t^a)_{ij} \gamma^\mu$

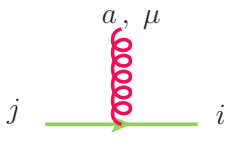

three-gluon: $\Gamma^{abc}_{\alpha\beta\gamma}(p,q,r) = -i\, g_s\, (F^a)_{bc}\, V_{\alpha\beta\gamma}(p,q,r)$

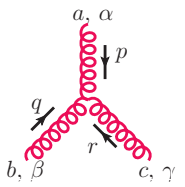

$$V_{\alpha\beta\gamma}(p,q,r) = (p-q)_\gamma g_{\alpha\beta} + (q-r)_\alpha g_{\beta\gamma} + (r-p)_\beta g_{\alpha\gamma}\,, \quad p^\alpha + q^\alpha + r^\alpha = 0$$

four-gluon: $\Gamma^{abcd}_{\alpha\beta\gamma\delta} = -i\,g_s^2 \begin{bmatrix} +f^{xac}\,f^{xbd}\,(g_{\alpha\beta}g_{\gamma\delta} - g_{\alpha\delta}g_{\beta\gamma}) \\ +f^{xad}\,f^{xcb}\,(g_{\alpha\gamma}g_{\beta\delta} - g_{\alpha\beta}g_{\gamma\delta}) \\ +f^{xab}\,f^{xdc}\,(g_{\alpha\delta}g_{\beta\gamma} - g_{\alpha\gamma}g_{\beta\delta}) \end{bmatrix}$

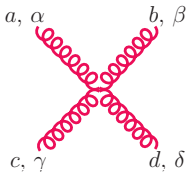

ghost–gluon: $\Gamma^{\mu,\,a}_{g\eta\bar{\eta}} = -i\,g_s\,(F^a)_{bc}\,p^\mu$

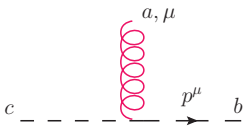

External lines are represented by the spinors for incoming and outgoing fermions with momentum p and spin s and polarisation vectors for vector bosons with polarisation λ (see Fig. 14).

- outgoing fermion: $\bar{u}(p,s)$
- incoming fermion: $u(p,s)$
- outgoing vector boson: $\epsilon^*_\mu(p,\lambda)$
- outgoing antifermion: $v(p,s)$
- incoming antifermion: $\bar{v}(p,s)$
- incoming vector boson: $\epsilon_\mu(p,\lambda)$.

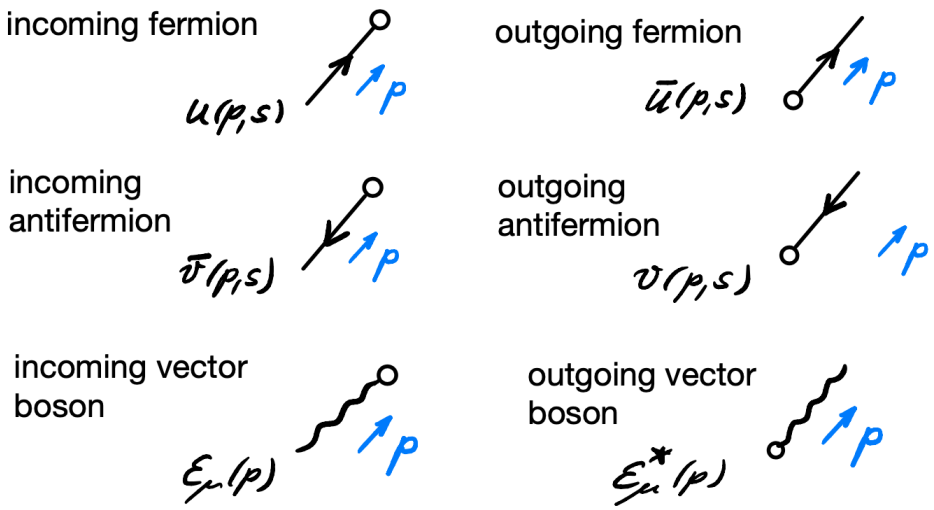

Fig. 14: Conventions for spinors with momentum p and spin s and polarisation vectors $\epsilon_\mu(p,\lambda)$.

3 Amplitudes and cross sections

3.1 Tree-level amplitudes

3.1.1 Partonic cross sections

The partonic cross section $\hat{\sigma}_{ij}$ in eq. (2) can be calculated order by order in perturbation theory. It contains the modulus of the scattering or decay matrix element, $|\mathcal{M}|^2$, which encodes the fundamental interactions derived from the Lagrangian.

For a reaction $p_i + p_j \to p_1 + \ldots + p_n$, the reaction rate can be calculated according to Fermi's golden rule based on the transition matrix element $|\mathcal{M}|^2$. We have

$$\begin{aligned} \mathrm{d}\hat{\sigma} &= \frac{J}{\text{flux}} \cdot |\mathcal{M}|^2 \cdot \mathrm{d}\Phi_n \,, \\ \text{flux} &= 4\sqrt{(p_i \cdot p_j)^2 - m_i^2 m_j^2} \,. \end{aligned} \tag{51}$$

Assuming massless incoming particles and calculating in the centre-of-mass frame of $p_i + p_j$, we find $\text{flux} = 4p_i \cdot p_j = 2\hat{s}$, with $\hat{s} = (p_i + p_j)^2$. The quantity $J = 1/j!$ is a statistical factor to be included for each group of j identical particles in the final state. The phase-space volume spanned by the final-state particles is denoted by $\mathrm{d}\Phi_n$, it will be considered in more detail in section 4.1.

For a decay process $Q \to p_1 + \ldots + p_n$ we have

$$\mathrm{d}\Gamma = \frac{J}{2\sqrt{Q^2}} \cdot |\mathcal{M}|^2 \cdot \mathrm{d}\Phi_n \,. \tag{52}$$

If the polarisations or spins of the final state particles are not measured, we sum over all possible polarisations/spins in the final state. Colour in the final state cannot be measured, so we also have to sum over all colours in the final state. Furthermore, we average over all possible colours, polarisations and spins in the initial state. The matrix element is then given by

$$|\mathcal{M}|^2 \to \overline{\sum}|\mathcal{M}|^2 = \left(\prod_{\text{initial}} \frac{1}{N_{\text{pol}} N_{\text{col}}} \right) \sum_{\text{pol,col}} |\mathcal{M}|^2 \,, \tag{53}$$

where for quarks $N_{\text{col}} = N_c$, for gluons $N_{\text{col}} = N_c^2 - 1$, and $N_{\text{pol}} = 2$ for both, quarks and gluons, as long as we stay in four space–time dimensions. The expression $\overline{\sum}|\mathcal{M}|^2$ is often just written as $|\overline{\mathcal{M}}|^2$.

3.1.2 Total hadronic cross section

For hadron colliders, the cross section σ at a centre-of-mass energy $\sqrt{s}$ can be expressed in terms of the partonic cross section and a luminosity function

$$\mathcal{L}_{ij}(x_1, x_2, \mu_f) = f_{i/p_a}(x_1, \mu_f) f_{j/p_b}(x_2, \mu_f) \,, \tag{54}$$

where $f_i(x, \mu_f)$ is the parton distribution function of a parton with momentum fraction x and flavour i (including gluons) and μ_f is the factorisation scale, such that

$$\begin{aligned} \sigma(s) &= \int_{\hat{s}_{min}}^{s} \mathrm{d}\hat{s} \int_0^1 \mathrm{d}x_1 \int_0^1 \mathrm{d}x_2 \, \delta(\hat{s} - x_1 x_2 s) \sum_{i,j} \mathcal{L}_{ij}(x_1, x_2, \mu_f) \int \mathrm{d}\hat{\sigma}_{ij}(x_1, x_2, \mu_r, \mu_f) \\ &= \int_{\tau_{min}}^1 \mathrm{d}\tau \int_\tau^1 \frac{\mathrm{d}x}{x} \sum_{ij} f_i(x, \mu_f) \, f_j(\frac{\tau}{x}, \mu_f) \, \sigma_{ij}(\hat{s} = \tau s) \end{aligned} \tag{55}$$

In the second line the replacement $x_{1,2} = \sqrt{\tau} e^{\pm y}$, $\mathrm{d}x_1 \mathrm{d}x_2 = \mathrm{d}\tau \mathrm{d}y$ has been made.

3.2 Running couplings and masses

In this section we would like to explain how it arises that theoretical predictions depend in general on at least one unphysical scale, the so-called *renormalisation scale* μ. In the case of hadronic initial-state particles, there is also a *factorisation scale* μ_f involved. There can be even more unphysical scales, like fragmentation scales in the modelling of the fragmentation of final-state particles into hadrons, parton shower matching scales, or resummation scales.

Let us first motivate how the dependence on a renormalisation scale arises. We mentioned already that the strong coupling, defined as $\alpha_s = g_s^2/(4\pi)$, is not really a constant. To leading order in the perturbative expansion, it obeys the relation

$$\alpha_s(Q^2) = \frac{\alpha_s(\mu^2)}{1 + b_0\, t\, \alpha_s(\mu^2)} \quad , \quad ; t = \ln \frac{Q^2}{\mu^2} \, . \tag{56}$$

where Q^2 is a generic energy scale, for example the centre-of-mass energy of a scattering process. The coefficient b_0 is given by

$$b_0 = \frac{1}{4\pi} \left(\frac{11}{3} C_A - \frac{4}{3} T_R N_F \right) \, , \tag{57}$$

where N_F is the number of flavours in the quark loops contributing to the gluon self-energy. Note that $b_0 > 0$ for $N_F < 11/2\, C_A$.

Where does the running of the coupling come from? It is closely linked to renormalisation, which introduces the *renormalisation scale* μ. Before we enter into the technicalities, let us look at a physical observable, for example the R-ratio which we encountered already,

$$R(s) = \frac{\sigma(e^+e^- \to \text{ hadrons})}{\sigma(e^+e^- \to \mu^+\mu^-)} \, , \tag{58}$$

assuming that the energy exchanged in the scattering process is much larger than Λ_{QCD}.

To get a precise result, we should include quantum corrections, for example diagrams where virtual gluons are exchanged, such as the ones shown in Fig. 15. The perturbative expansion for R can be written as

$$\begin{aligned} R(s) &= K_{QCD}(s)\, R_0 \, , \quad R_0 = N_c \sum_f Q_f^2\, \theta(s - 4m_f^2) \, , \\ K_{QCD}(s) &= 1 + \frac{\alpha_s(\mu^2)}{\pi} + \sum_{n \geq 2} C_n \left(\frac{s}{\mu^2} \right) \left(\frac{\alpha_s(\mu^2)}{\pi} \right)^n \, . \end{aligned} \tag{59}$$

The coefficients C_n can be calculated perturbatively, see e.g. Refs. [7, 52, 61] for results of order α_s^4 (five loops).

However, when trying to perform the loop integrals over a loop momentum k, we will find that they diverge for $k \to \infty$ in 4 space–time dimensions (see Section 3.4.1), therefore we need to introduce a regulator to be able to calculate them at all; usually dimensional regularisation is employed, calculating the integrals in $D = 4 - 2\epsilon$ space–time dimensions. For the argument to make here we instead use an arbitrary cutoff scale Λ_{UV} for the upper integration boundary. If we carried through the calculation, we

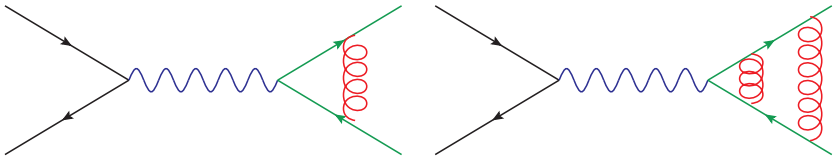

Fig. 15: Examples of one- and two-loop diagrams contributing to $e^+e^- \to q\bar{q}$.

would see that the dependence on the cutoff in the left diagram of Fig. 15 cancels, which is a consequence of the Ward Identity. However, if we go one order higher in α_s, calculating diagrams like the one on the right-hand side in Fig. 15, the cutoff-dependence does not cancel anymore. We obtain

$$K_{QCD}(s) = 1 + \frac{\alpha_s}{\pi} + \left(\frac{\alpha_s}{\pi}\right)^2 \left[c + b_0 \pi \, \log\left(\frac{\Lambda_{UV}^2}{s}\right)\right] + \mathcal{O}(\alpha_s^3) \,, \tag{60}$$

where c is a constant. So our result is infinite as we take the limit $\Lambda_{UV} \to \infty$. However, we did not claim that α_s is the coupling we measure. In fact, it is the "bare" coupling, also denoted as α_s^0, which appears in Eq. (60), and we can absorb the infinity in the bare coupling to arrive at the renormalised coupling, which is identified with the one we measure. In our case, this looks as follows. We define

$$\alpha_s(\mu) = \alpha_s^0 + b_0 \log\left(\frac{\Lambda_{UV}^2}{\mu^2}\right) \alpha_s^2 \,, \tag{61}$$

then replace α_s^0 by $\alpha_s(\mu)$ and drop consistently all terms of order α_s^3. In other words, the divergence arising in the bare coupling α_s^0 when calculating quantum corrections is cancelled by the second term, the *counter term*. This leads to

$$K_{QCD}^{\text{ren}}(\alpha_s(\mu), \mu^2/s) = 1 + \frac{\alpha_s(\mu)}{\pi} + \left(\frac{\alpha_s(\mu)}{\pi}\right)^2 \left[c + b_0 \pi \, \log\left(\frac{\mu^2}{s}\right)\right] + \mathcal{O}(\alpha_s^3) \,. \tag{62}$$

K_{QCD}^{ren} is finite, but now it depends on the scale μ, both explicitly and implicitly through $\alpha_s(\mu)$. However, the hadronic R-ratio is a physical quantity and therefore cannot depend on the arbitrary scale μ. The dependence of K_{QCD} on μ is an artefact of the truncation of the perturbative series after the order α_s^2.

Renormalisation group and asymptotic freedom

Since the hadronic R-ratio $R^{\text{ren}} = R_0 \, K_{QCD}^{\text{ren}}$ cannot depend on μ (if it was calculated to all orders in perturbation theory), its total derivative w.r.t. μ must vanish:

$$\mu^2 \frac{\mathrm{d}}{\mathrm{d}\mu^2} R^{\text{ren}}(\alpha_s(\mu), \mu^2/Q^2) = 0 = \left(\mu^2 \frac{\partial}{\partial \mu^2} + \mu^2 \frac{\partial \alpha_s}{\partial \mu^2} \frac{\partial}{\partial \alpha_s}\right) R^{\text{ren}}(\alpha_s(\mu), \mu^2/Q^2) \,. \tag{63}$$

Equation (63) is an example of a so-called *renormalisation group equation (RGE)*. Introducing the abreviations

$$t = \ln \frac{Q^2}{\mu^2} \,, \qquad \beta(\alpha_s) = \mu^2 \frac{\partial \alpha_s}{\partial \mu^2} \,, \tag{64}$$

the RGE becomes

$$\left(-\frac{\partial}{\partial t} + \beta(\alpha_s) \frac{\partial}{\partial \alpha_s}\right) R^{\text{ren}} = 0 \,. \tag{65}$$

This first-order partial differential equation can be solved by implicitly defining a function $\alpha_s(Q^2)$, the *running coupling*, such that

$$t = \int_{\alpha_s}^{\alpha_s(Q^2)} \frac{\mathrm{d}x}{\beta(x)}\,, \quad \text{with} \quad \alpha_s \equiv \alpha_s(\mu^2)\,, \tag{66}$$

where μ^2 above is fixed to an arbitrary value. We can solve Eq. (66) perturbatively using an expansion of the β-function

$$\beta(\alpha_s) = -b_0\alpha_s^2\left[1 + \sum_{n=1}^{\infty} b_n\,\alpha_s^n\right], \tag{67}$$

where $b_0 = \frac{\beta_0}{4\pi}$ and $b_0 b_1 = \frac{\beta_1}{(4\pi)^2}$, etc. Explicitly, up to NNLO:

$$\mu^2\frac{\mathrm{d}\alpha_s(\mu)}{\mathrm{d}\mu^2} = -\alpha_s(\mu)\left[\beta_0\left(\frac{\alpha_s(\mu)}{2\pi}\right) + \beta_1\left(\frac{\alpha_s(\mu)}{2\pi}\right)^2 + \beta_2\left(\frac{\alpha_s(\mu)}{2\pi}\right)^3 + \mathcal{O}(\alpha_s^4)\right].$$

The four-loop coefficients are known since some time [76], the β-function at five loops has been calculated only recently [7, 22, 28, 52, 61]. The first three coefficients (in the $\overline{\text{MS}}$-scheme) are

$$\begin{aligned}
\beta_0 &= \frac{11\,C_A - 4T_R N_F}{6}\,,\\
\beta_1 &= \frac{17\,C_A^2 - 10C_A T_R N_F - 6C_F T_R N_F}{6}\,,\\
\beta_2 &= \frac{1}{432}\big(2857C_A^3 + 108C_F^2 T_R N_F - 1230C_F C_A T_R N_F - 2830C_A^2 T_R N_F\\
&\quad + 264C_F T_R^2 N_F^2 + 316C_A T_R^2 N_F^2\big)\,.
\end{aligned} \tag{68}$$

Truncating the series Eq. (67) at leading order leads to the simple solution given already in Eq. (56),

$$\begin{aligned}
Q^2\,\frac{\partial\alpha_s}{\partial Q^2} = \frac{\partial\alpha_s}{\partial\, t} = -b_0\alpha_s^2 \;&\Rightarrow\; -\frac{1}{\alpha_s(Q^2)} + \frac{1}{\alpha_s(\mu^2)} = -b_0\,t\\
&\Rightarrow\; \alpha_s(Q^2) = \frac{\alpha_s(\mu^2)}{1 + b_0\,t\,\alpha_s(\mu^2)}\,.
\end{aligned} \tag{69}$$

Eq. (69) implies that

$$\alpha_s(Q^2) \overset{Q^2\gg\mu^2}{\longrightarrow} \frac{1}{b_0 t} \overset{Q^2\to\infty}{\longrightarrow} 0\,. \tag{70}$$

This behaviour is called *asymptotic freedom*: the larger Q^2, the smaller the coupling, so at very high energies (small distances), the quarks and gluons can be treated as if they were free particles. The behaviour of α_s as a function of Q^2 is illustrated in Fig. 16 including measurements at different energies. Note that the sign of b_0 is positive for QCD (see eq. (57)), while its analogue in QED is negative. The decrease of the coupling $\alpha_s(Q^2)$ with increasing Q^2 can be related to "screening and anti-screening" effects of colour charges, to be contrasted to the screening of electric charges due to vacuum polarisation in the QED case. The gluon loops, leading to the C_A-term in b_0, have the opposite sign relative to the quark loops, and the effect of the gluon loops is dominating: the positive term in b_0 is larger than the negative term. It can be proven that, in four space–time dimensions, only non-Abelian gauge theories

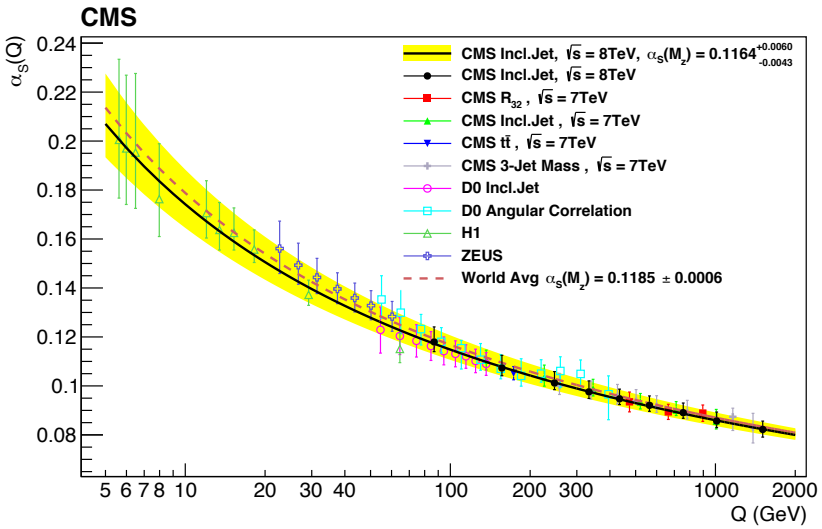

Fig. 16: The running coupling $\alpha_s(Q^2)$. Figure from Ref. [54].

can be asymptotically free. For the discovery of asymptotic freedom in QCD [47, 69], Gross, Politzer, and Wilczek got the Nobel Prize (much later, in 2004).

The QCD Λ-parameter

Instead of the arbitrary scale μ in Eq. (66) one can also use a characteristic scale, the scale where the coupling would diverge or at least becomes so strong that perturbation theory makes no sense anymore. This scale is the QCD Λ-parameter. It is defined by

$$\log\left(\frac{Q^2}{\Lambda^2_{QCD}}\right) = -\int_{\alpha_s(Q^2)}^{\infty}\frac{\mathrm{d}x}{\beta(x)} = \int_{\alpha_s(Q^2)}^{\infty}\frac{\mathrm{d}x}{b_0x^2(1+b_1x+\ldots)} \tag{71}$$

Keeping only the leading term we find the familiar form

$$\alpha_s(Q^2) = \frac{1}{b_0\log\left(Q^2/\Lambda^2_{QCD}\right)}\,, \tag{72}$$

Using $L = \log(Q^2/\Lambda^2_{QCD})$ yields the following solution up to NNLO,

$$\alpha_s(Q^2) = \frac{4\pi}{\beta_0 L}\left(1 - \frac{\beta_1}{\beta_0^2}\frac{\log L}{L} + \frac{1}{\beta_0^2L^2}\left(\frac{\beta_1^2}{\beta_0^2}\left(\log^2 L - \log L - 1\right) + \frac{\beta_2}{\beta_0}\right)\right)\,. \tag{73}$$

Note that Λ_{QCD} depends on the number of flavours because $N_F = 4$ for $m_c < Q < m_b$, $N_F = 5$ for $m_b < Q < m_t$, etc.

Running quark masses

In the derivation of the RGE in Eq. (63) above, we have assumed that the observable R does not depend on other couplings or parameters, such as quark masses. However, if the considered observable depends

on masses, the latter also require renormalisation. Introducing the renormalisation constant Z_m, we have

$$\begin{aligned} &\mu \frac{d\, m^{(0)}}{d\mu} = 0 \;,\; m^{(0)} = Z_m\, m \\ &\Rightarrow \mu\, \frac{d\, Z_m}{d\mu} \cdot m + \mu \cdot Z_m \frac{dm}{d\mu} = 0 \;. \end{aligned} \tag{74}$$

The *mass anomalous dimension* γ_m is defined by

$$\mu^2 \frac{\partial m}{\partial \mu^2} = -\gamma_m(\alpha_s(\mu^2))\, m(\mu^2) \;, \tag{75}$$

where the minus sign pulled out in front of γ_m is convention.

This naturally leads to renormalisation group equations that are extended to include mass renormalisation, which will lead to running quark masses:

$$\left(\mu^2 \frac{\partial}{\partial \mu^2} + \beta(\alpha_s) \frac{\partial}{\partial \alpha_s} - \gamma_m(\alpha_s) m \frac{\partial}{\partial\, m}\right) R\left(\frac{Q^2}{\mu^2}, \alpha_s, \frac{m}{Q}\right) = 0 \;. \tag{76}$$

In a perturbative expansion we can write the mass anomalous dimension as

$$\gamma_m(\alpha_s) \;=\; c_0\, \alpha_s \left(1 + \sum_n c_n \alpha_s^n\right) \;.$$

The coefficients are known up to c_4, i.e. $\mathcal{O}(\alpha_s^5)$ [5,6,49,60].

Even though the top quark mass is not an observable, a more commonly used renormalisation scheme for top quark masses is the on-shell renormalisation scheme, where the idea is to preserve the on-shell mass of a particle, which corresponds to the zero of the real part of the inverse propagator. However, the on-shell mass of the top quark suffers from so-called renormalon contributions, which affect the convergence properties of the perturbative expansion. The conversion between the pole mass M_t and the $\overline{\text{MS}}$ mass $m_t(\mu_m)$ is given by [18]

$$M_t = m_t(\mu_m)\, d(m_t(\mu_m), \mu_m) = m_t(\mu_m) \left(1 + \sum_{k=1}^{\infty} \left(\frac{\alpha_s(\mu_m)}{\pi}\right)^k d^{(k)}(\mu_m)\right) . \tag{77}$$

The first two perturbative coefficients $d^{(1)}$ and $d^{(2)}$ in Eq. (77) have the values [37,44]

$$\begin{aligned} d^{(1)}(\mu_m) &= \frac{4}{3} + L_{\mu_m} \,, \\ d^{(2)}(\mu_m) &= \frac{307}{32} + 2\,\zeta_2 + \frac{2}{3}\,\zeta_2\,\ln 2 - \frac{1}{6}\,\zeta_3 + \frac{509}{72}\,L_{\mu_m} + \frac{47}{24}\,L_{\mu_m}^2 \\ &\quad - \left(\frac{71}{144} + \frac{1}{3}\,\zeta_2 + \frac{13}{36}\,L_{\mu_m} + \frac{1}{12}\,L_{\mu_m}^2\right) N_F \,, \end{aligned} \tag{78}$$

where

$$L_{\mu_m} = 2\ln(\mu_m / m_t(\mu_m)) \,. \tag{79}$$

Higher-order coefficients were computed in Refs. [23,36,63,66].

3.3 Scale uncertainties

Let us consider an observable O, calculated in perturbation theory to order α_s^{N+k},

$$O = \sum_{n=0}^{N} C_n(\mu_r)\alpha_s^{n+k}(\mu_r) \ ,$$

where k is the power of α_s of the leading order cross section. From the perturbative solution of the RGE we can derive how the physical quantity $O^{(N)}(\mu)$, truncated at order N in perturbation theory, changes with the renormalisation scale μ:

$$\frac{\mathrm{d}}{\mathrm{d}\log(\mu^2)} O^{(N)}(\alpha_s(\mu)) = \beta(\alpha_s)\frac{\partial O^{(N)}}{\partial \alpha_s} \sim \mathcal{O}\left(\alpha_s^{N+1}(\mu)\right) \ , \tag{80}$$

where the order $\alpha_s^{N+1}(\mu)$ arises because $\beta(\alpha_s) = -b_0\alpha_s^2 + \mathcal{O}(\alpha_s^3)$. This means that, the more higher-order coefficients C_n we can calculate, the weaker the dependence of the result on the unphysical scale μ^2 will be. Therefore, the dependence on the scale is used to estimate the uncertainty of a result stemming from missing higher orders. Usually the scale is varied by a factor of two up and down.

In hadronic collisions there is another scale, the factorisation scale μ_f, which comes from the factorisation of initial-state infrared singularities. It also needs to be taken into account when assessing the uncertainty of a theoretical prediction. Varying both μ_r and μ_f simultaneously in the same direction can lead to accidental cancellations and hence an underestimation of the perturbative uncertainties. Therefore, in the presence of both μ_r and μ_f, usually so-called *7-point scale variations* are performed, which means $\mu_{r,f} = c_{r,f}\mu_0$, where $c_r, c_f \in \{2, 1, 0.5\}$ and where the extreme variations $(c_r, c_f) = (2, 0.5)$ and $(c_r, c_f) = (0.5, 2)$ have been omitted.

Still, the question remains what to choose for the central scale μ_0. A convenient choice is a scale where the higher-order corrections are small, i.e. a scale showing good "perturbative stability".

Let us now look at a few examples where such scale variations do not capture the true uncertainties. First some prelimiary remarks. If there is only one scale μ involved, the scale dependence of an observable is given through $\alpha_s(\mu)$, and we can use the renormalisation group equation to move from the result at a scale μ_0 to a result at a different scale. For the observable O, known to order α_s^{N+k}, we can use the requirement $\mathrm{d}O/\mathrm{d}\ln\left(\frac{\mu_r^2}{\mu_0^2}\right) = 0$ and Eq. (67) to derive how O changes with a change of scale, leading to

$$O = \alpha_s^k(\mu_r)\left\{C_0 + \left(C_1 + b_0 C_0 \ln\left(\frac{\mu_r^2}{\mu_0^2}\right)\right)\alpha_s(\mu_r) + \mathcal{O}(\alpha_s^2)\right\} \ . \tag{81}$$

Variations of μ_r will change the C_0-part of the $\mathcal{O}(\alpha_s^{k+1})$ term, however the magnitude of C_1 can only be determined by direct calculation.

For some processes, C_1 (and C_2) turned out to be pretty large, and the scale uncertainty bands obtained from 7-point scale variations do not (fully) overlap between the different orders. One such example is Higgs production in gluon fusion, known to order N^{3}LO. Figure 17 (left) shows a slow stabilisation of the scale dependence with increasing perturbative order, and the higher-order corrections are very large. The standard scale uncertainty bands are shown in Fig. 17 (right). It is obvious that

the LO scale variation band would be a very poor measure of the uncertainty due to missing higher orders. Among the reasons for the large K-factors (i.e. the relative size of the higher-order corrections), in particular the NLO K-factor, are large colour factors and new partonic channels opening up. Furthermore, the behaviour of the scale uncertainty bands can depend sensitively on the definition of the central scale.

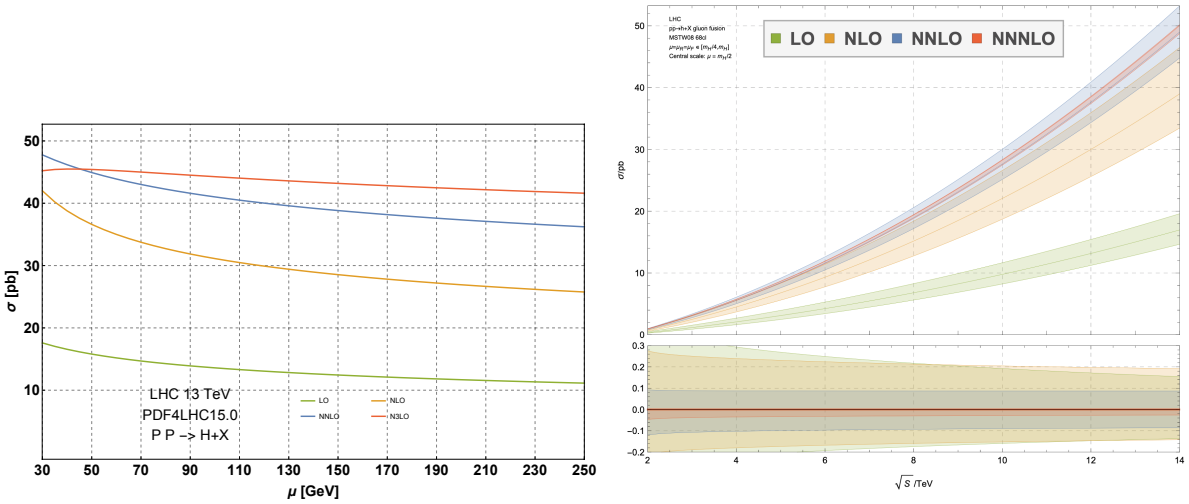

Fig. 17: Left: Higgs production in gluon fusion, stabilisation of the scale dependence. Figure from Ref. [67]. Right: Scale uncertainty bands for Higgs production in gluon fusion. Figure from Ref. [4].

Usually one can see that the perturbative series stabilises at latest between NNLO and N^{3}LO. However, there are exceptions as well, an example is charged-current Drell–Yan production, calculated to N^{3}LO in Refs. [15, 21, 34]. With a central scale of $Q = 100\,\text{GeV}$, NNLO PDFs and 7-point scale variations, the NNLO and N^{3}LO uncertainty bands do not overlap, see Fig. 18. Looking at the variation of the factorisation scale separately, the NNLO μ_f-uncertainty band is found to be accidentally small; this has been traced back to cancellations between different partonic channels.

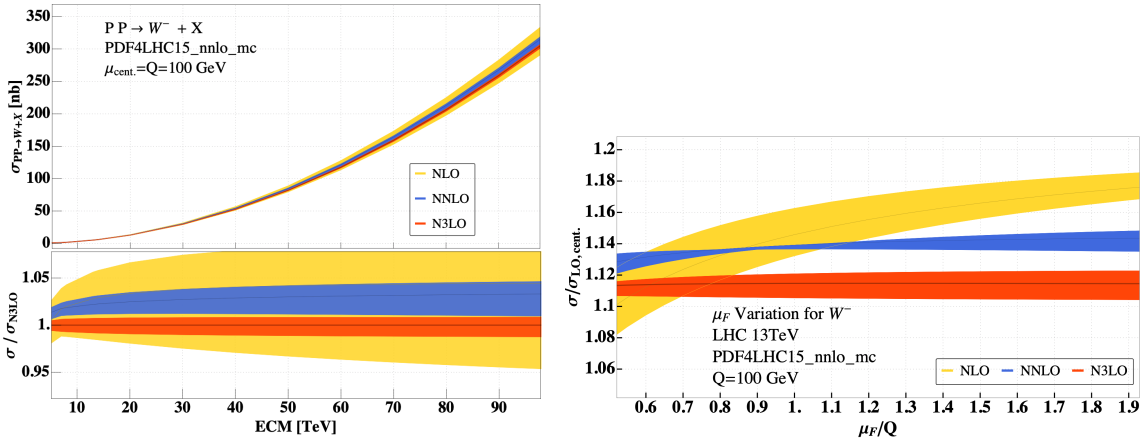

Fig. 18: Charged-current Drell–Yan production, left: cross section with scale bands for combined renormalisation and factorisation scale dependence. Right: factorisation scale dependence shown separately. Figure from Ref. [34].

3.4 Basics of NLO QCD calculations

3.4.1 Dimensional regularisation

Tree-level results in QCD are usually not accurate enough to match the current experimental precision and suffer from large scale uncertainties. When calculating higher orders, we encounter non-integrable singularities: ultraviolet (UV) singularities and infrared (IR) singularities, the latter are due to soft or collinear massless particles. Therefore the introduction of a *regulator* is necessary.

Let us first have a look at UV singularities: The expression for the one-loop two-point function shown in Fig. 19 naively would be

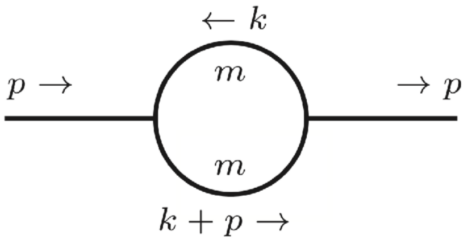

Fig. 19: One-loop two-point function I_2 ("bubble").

$$I_2 = \int_{-\infty}^{\infty} \frac{d^4k}{(2\pi)^4} \frac{1}{[k^2 - m^2 + i\delta][(k+p)^2 - m^2 + i\delta]} \,. \tag{82}$$

If we are only interested in the behaviour of the integral for $|k| \to \infty$ we can neglect the masses, transform to polar coordinates and obtain

$$I_2 \sim \int \mathrm{d}\Omega_3 \int_0^{\infty} \mathrm{d}|k| \frac{|k|^3}{|k|^4} \,. \tag{83}$$

This integral is clearly not well-defined. If we introduce an upper cutoff Λ (and a lower limit $|k|_{\min}$ because we neglected the masses and p^2, which would serve as an IR regulator), the integral is regulated:

$$I_2 \sim \int_{|k|_{\min}}^{\Lambda} \mathrm{d}|k| \frac{1}{|k|} \sim \log\left(\frac{\Lambda}{|k|_{\min}}\right) \,. \tag{84}$$

The integral has a logarithmic UV divergence for $\Lambda \to \infty$. The regularisation with a cut-off Λ is problematic since it is neither a Lorentz invariant nor a gauge invariant way to regulate integrals over loop momenta. A regularisation method which preserves these symmetries is *dimensional regularisation*.

Dimensional regularisation has been introduced in 1972 by 't Hooft and Veltman [74], and by Bollini and Giambiagi [12], as a method to regularise UV divergences in a gauge invariant way, thus completing the proof of renormalisability. The idea is to work in $D = 4 - 2\epsilon$ space–time dimensions. Divergences for $D \to 4$ will appear as poles in $1/\epsilon$. This means that objects such as momenta, polarisation vectors and the metric tensor live in a D-dimensional space. The γ-algebra also has to be extended to D dimensions, however, how to treat unphysical objects is not unique. There are several *regularisation schemes* within dimensional regularisation. For example, when doing a calculation in supersymmetry, it is inconvenient to use a scheme where massless bosons have $D - 2$ polarisation states while massless

fermions have two polarisation states. Of course, all the different schemes must lead to the same result for physical quantities.

An important feature of dimensional regularisation is that, apart from UV singularities, it also regulates IR singularities, i.e. divergences occurring when massless particles become soft and/or collinear. Ultraviolet divergences occur for loop momenta $k \to \infty$, so in general the UV behaviour becomes better for $\epsilon > 0$, while the IR behaviour gets better for $\epsilon < 0$. Certainly we cannot have $D < 4$ and $D > 4$ at the same time. What is formally done is to first assume the IR divergences are regulated in some other way, e.g. by assuming all external legs are off-shell or by introducing a small mass for all massless particles. In this case all poles in $1/\epsilon$ will be of UV nature and renormalisation can be performed. After renormalisation we can analytically continue to the whole complex D-plane, in particular to $\mathrm{Re}(D) > 4$. If we now remove the auxiliary IR regulator, the IR divergences will show up as $1/\epsilon$ poles (this is however not commonly done in practice, where all poles just show up as $1/\epsilon$ poles, and after UV renormalisation, the remaining poles must be of IR origin).

In dimensional regularisation, slight changes to the Feynman rules are to be made: we multiply the couplings in the Lagrangian by a factor μ^ϵ: $g \to g\mu^\epsilon$, where μ is an arbitrary mass scale. This ensures that each term in the Lagrangian has the correct mass dimension while retaining a dimensionless coupling in which we perform the perturbative expansion. The momentum integration involves $\int \frac{d^D k}{(2\pi)^D}$ for each loop.

We will not dive more deeply into the subject of loop calculations here, but rather discuss some general features of NLO calculations below.

4 Soft and collinear emissions, Jets

4.1 Cancellation of infrared singularities

Next-to-leading order calculations consist of several parts, which can be classified as virtual corrections (containing usually one loop), real corrections (radiation of extra particles relative to the leading order), and subtraction terms to deal with singularities. In the following we will assume that the virtual corrections already include UV renormalisation, such that the subtraction terms only concern the subtraction of the infrared (IR) singularities. IR singularities occur when a massless particle becomes soft (low energy) or when two massless particles become collinear to each other.

We will consider the next-to-leading order in an expansion in the strong coupling constant α_s. For electroweak corrections, the general structure is similar. The real and virtual contributions to the simple example $\gamma^* \to q\bar{q}$ (the hadronic part of $e^+e^- \to q\bar{q}$) are shown in Fig. 20.

If $\mathcal{M}_0$ is the leading-order amplitude and $\mathcal{M}_{\mathrm{virt}}, \mathcal{M}_{\mathrm{real}}$ are the virtual and real NLO amplitudes as shown in Fig. 20, the corresponding cross section is given by

$$\sigma^{NLO} = \underbrace{\int \mathrm{d}\phi_2 \, |\mathcal{M}_0|^2}_{\sigma^{LO}} + \int_R \mathrm{d}\phi_3 \, |\mathcal{M}_{\mathrm{real}}|^2 + \int_V \mathrm{d}\phi_2 \, 2\mathrm{Re}\left(\mathcal{M}_{\mathrm{virt}} \mathcal{M}_0^*\right) \ . \tag{85}$$

The sum of the integrals $\int_R$ and $\int_V$ above is finite. However, this is not true for the individual contributions. The real part contains divergences due to soft and collinear radiation of massless particles. While

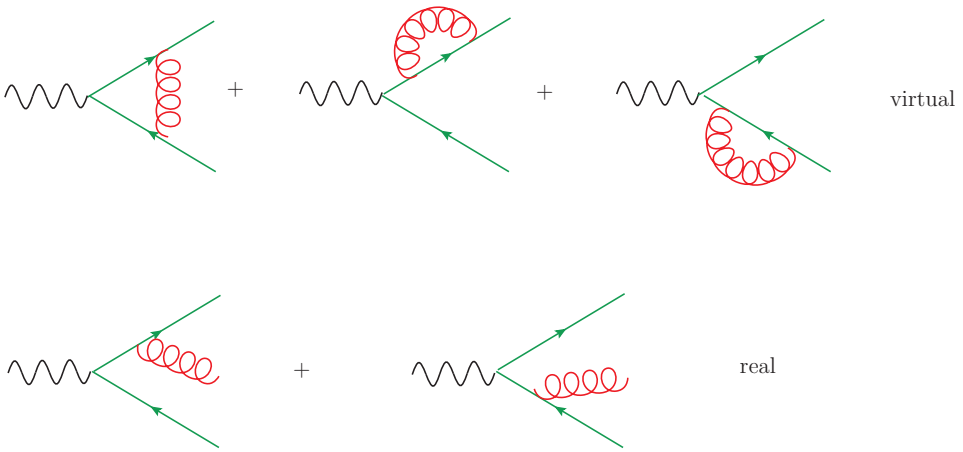

Fig. 20: The real and virtual NLO QCD contributions to $\gamma^* \to q\bar{q}$.

$\mathcal{M}_{\text{real}}$ itself is a tree level amplitude and thus finite, the divergences show up upon integration over the phase space $\mathrm{d}\Phi_3$. In $\int_V$, the phase space is the same as for the Born amplitude, but the loop integrals in $\mathcal{M}_{\text{virt}}$ contain explicit IR singularities.

Let us anticipate the answer, which we will (partly) calculate later. We find:

$$\sigma_R = \sigma^{\text{Born}} \tilde{H}(\epsilon)\, C_F \frac{\alpha_s}{2\pi} \left(\frac{2}{\epsilon^2} + \frac{3}{\epsilon} + \frac{19}{2} \right) , \tag{86}$$
$$\sigma_V = \sigma^{\text{Born}} H(\epsilon)\, C_F \frac{\alpha_s}{2\pi} \left(-\frac{2}{\epsilon^2} - \frac{3}{\epsilon} - 8 \right) ,$$

where $H(\epsilon) = \left(\frac{4\pi\mu^2}{-Q^2}\right)^{\epsilon} \frac{\Gamma(1+\epsilon)\Gamma^2(1-\epsilon)}{\Gamma(1-2\epsilon)}$ and $\tilde{H}(\epsilon) = H(\epsilon) + \mathcal{O}(\epsilon^3)$. The exact ϵ-dependence of $H(\epsilon) = 1 + \mathcal{O}(\epsilon)$ is irrelevant after summing up real and virtual contributions, because the poles in ϵ all cancel. This must be the case according to the **KLN theorem** (Kinoshita–Lee–Nauenberg) [55, 58]. It says that

IR singularities must cancel when summing the transition rate over all degenerate (initial and final) states.

In our example, we do not have initial state singularities. However, in the final state we can have a massless quark accompanied by a soft gluon, or a collinear quark–gluon pair. Such a state cannot be distinguished from just a quark state, and therefore these two configurations are "degenerate". Only when summing over all the final-state multiplicities contributing to the cross section at a given order in α_s, the divergences cancel. Another way of stating this is by looking at the squared amplitude at order α_s and considering all cuts, see Fig. 21 (self-energy contributions, which are zero for massless quarks, are not shown). The KLN theorem states that *the sum of all diagrams resulting from cuts that lead to physical final states is free of IR poles.*

The cancellations between $\int_R$ and $\int_V$ in Eq. (85) are non-trivial, because the phase-space integrals contain a different number of particles in the final state and are thus of different dimensionality.

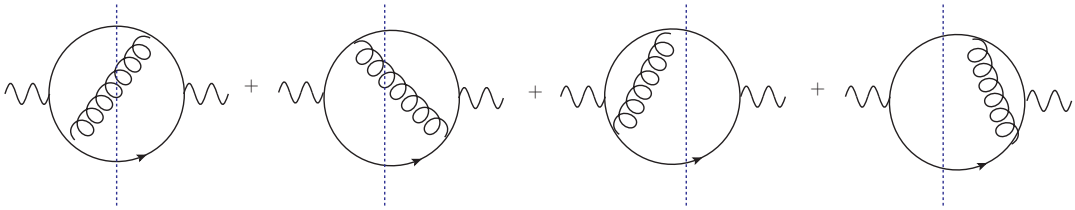

Fig. 21: The sum over cuts of the amplitude squared shown above is finite according to the KLN theorem.

Infrared safety

If we want to calculate a prediction for a certain observable, based on an n-particle final state, we need to multiply the amplitude by a *measurement function* $J(p_1 \dots p_n)$. The measurement function can contain for example a jet definition, or the definition of an event shape observable, or it defines observables such as the transverse momentum distribution of a final state particle. Schematically, the structure of the NLO cross section is the following. In the real radiation part, we have $n+1$ particles in the final state. Therefore the measurement function for the real radiation part depends on $n+1$ particles, while for the Born and virtual parts it only depends on n particles. Let us consider the case where we have an IR pole if the variable x, describing for example the energy of an extra gluon with momentum p_{n+1} in the real radiation part, goes to zero. If we define

$$\begin{aligned}
\mathcal{B}_n &= \int \mathrm{d}\phi_n \, |\mathcal{M}_0|^2 = \int \mathrm{d}\phi_n B_n \\
\mathcal{V}_n &= \int \mathrm{d}\phi_n \, 2\mathrm{Re}\left(\mathcal{M}_{\mathrm{virt}}\mathcal{M}_0^*\right) = \int \mathrm{d}\phi_n \frac{V_n}{\epsilon} \\
\mathcal{R}_n &= \int \mathrm{d}\phi_{n+1} \, |\mathcal{M}_{\mathrm{real}}|^2 = \int \mathrm{d}\phi_n \int_0^1 \mathrm{d}x \, x^{-1-\epsilon} \, R_n(x)
\end{aligned} \tag{87}$$

and a measurement function $J(p_1 \dots p_n, p_{n+1})$ we have

$$\sigma^{NLO} = \int \mathrm{d}\phi_n \left\{ \left(B_n + \frac{V_n}{\epsilon} \right) J(p_1 \dots p_n, 0) + \int_0^1 \mathrm{d}x \, x^{-1-\epsilon} \, R_n(x) \, J(p_1 \dots p_{n+1}) \right\} . \tag{88}$$

In the inclusive case (calculation of the total cross section) we have $J \equiv 1$. The integration over x leads to the explicit $1/\epsilon$ poles which must cancel with the virtual part:

$$\int_0^1 \mathrm{d}x \, x^{-1-\epsilon} \, R_n(x) = -\frac{R_n(0)}{\epsilon} + \int_0^1 \mathrm{d}x \, x^{-\epsilon} \frac{R_n(x) - R_n(0)}{x} . \tag{89}$$

The cancellation of the poles between $\frac{V_n}{\epsilon}$ and $\frac{R_n(0)}{\epsilon}$ in the non-inclusive case will only work if

$$\lim_{p_{n+1} \to 0} J(p_1 \dots p_n, p_{n+1}) = J(p_1 \dots p_n, 0) . \tag{90}$$

This is a non-trivial condition for the definition of an observable, for example a jet algorithm, and is called *infrared safety*. The formulation above is taylored to the soft limit where all components of p_{n+1} go to zero, however, an analogous condition must hold if two momenta become collinear.

As mentioned above, the measurement function is also important if we define differential cross

sections $\mathrm{d}\sigma/\mathrm{d}X$. In this case we have $J(p_1 \dots p_n) = \delta(X - \chi_n(p_i))$, where $\chi_n(p_i)$ is the definition of the observable, based on n partons. Again, infrared safety requires $\chi_{n+1} \to \chi_n$ if one of the p_i becomes soft or two of the momenta become collinear to each other.

Phase space integrals in D dimensions

To see how the cancellation works for *inclusive* quantities such as the total cross section, let us consider the real radiation contribution to $e^+e^- \to 2\,$jets at NLO in more detail. For this purpose we need phase space integrals in D dimensions.

The general formula for a $1 \to n$ particle phase space $\mathrm{d}\Phi_n$ with $Q \to p_1 \dots p_n$ is given by

$$\mathrm{d}\Phi_{1\to n} = (2\pi)^{n-D(n-1)} \Big[\prod_{j=1}^{n} d^D p_j \delta(p_j^2 - m_j^2)\Theta(E_j)\Big] \delta\Big(Q - \sum_{i=1}^{n} p_i\Big) \,. \tag{91}$$

In the following we will stick to the massless case $m_j = 0$. We use

$$d^D p_j \delta(p_j^2)\Theta(E_j) = dE_j d^{D-1}\vec{p}_j \delta(E_j^2 - \vec{p}_j^{\,2})\Theta(E_j) = \frac{1}{2E_j} d^{D-1}\vec{p}_j \Big|_{E_j = |\vec{p}_j|} \tag{92}$$

for $j = 1, \dots, n-1$ to arrive at

$$\mathrm{d}\Phi_{1\to n} = (2\pi)^{n-D(n-1)} 2^{1-n} \prod_{j=1}^{n-1} \frac{\mathrm{d}^{D-1}\vec{p}_j}{|\vec{p}_j|} \delta\Big((Q - \sum_{i=1}^{n-1} p_i)^2\Big) \,, \tag{93}$$

where we have used the last δ-function in Eq. (91) to eliminate p_n. We further use

$$\frac{\mathrm{d}^{D-1}\vec{p}}{|\vec{p}|} f(|\vec{p}|) = \mathrm{d}\Omega_{D-2}\, \mathrm{d}|\vec{p}|\, |\vec{p}|^{D-3} f(|\vec{p}|) \,, \tag{94}$$

$$\int \mathrm{d}\Omega_{D-2} = \int \mathrm{d}\Omega_{D-3} \int_0^\pi \mathrm{d}\theta (\sin\theta)^{D-3} = \int_0^\pi \mathrm{d}\theta_1 (\sin\theta_1)^{D-3} \int_0^\pi \mathrm{d}\theta_2 (\sin\theta_2)^{D-4} \dots \int_0^{2\pi} d\theta \,,$$

to obtain

$$\mathrm{d}\Phi_{1\to n} = (2\pi)^{n-D(n-1)} 2^{1-n} \left(\prod_{j=1}^{n-1} \mathrm{d}\Omega_{D-1-j}\, \mathrm{d}|\vec{p}_j|\, |\vec{p}_j|^{D-3}\right) \delta\Big((Q - \sum_{i=1}^{n-1} p_i)^2\Big) \,. \tag{95}$$

Example* $\mathbf{1 \to 3}$*:

For $n = 3$ one can choose a coordinate frame such that

$$\begin{aligned} &Q = (E, \vec{0}^{(D-1)}) \,, \quad p_1 = E_1\,(1, \vec{0}^{(D-2)}, 1) \,, \\ &p_2 = E_2\,(1, \vec{0}^{(D-3)}, \sin\theta, \cos\theta) \,, \quad p_3 = Q - p_2 - p_1 \,, \end{aligned} \tag{96}$$

leading to

$$\mathrm{d}\Phi_{1\to 3} = \frac{1}{4}(2\pi)^{3-2\,D}\, \mathrm{d}E_1 \mathrm{d}E_2 \mathrm{d}\theta_1\, (E_1 E_2 \sin\theta)^{D-3}\, \mathrm{d}\Omega_{D-2}\, \mathrm{d}\Omega_{D-3}$$

$$\Theta(E_1)\,\Theta(E_2)\,\Theta(E-E_1-E_2)\,\delta((Q-p_1-p_2)^2)\;. \tag{97}$$

In the following a parametrisation in terms of the Mandelstam variables $s_{ij} = 2\,p_i\cdot p_j$ will be useful, therefore we make the transformation $E_1, E_2, \theta \to s_{12}, s_{23}, s_{13}$. To work with dimensionless variables we define $y_1 = s_{12}/Q^2$, $y_2 = s_{13}/Q^2$, $y_3 = s_{23}/Q^2$ which leads to

$$\begin{aligned}\mathrm{d}\Phi_{1\to3} = (2\pi)^{3-2\,D}\,2^{-1-D}(Q^2)^{D-3}\,\mathrm{d}\Omega_{D-2}\,\mathrm{d}\Omega_{D-3}\,\mathrm{d}y_1\,\mathrm{d}y_2\,\mathrm{d}y_3\\ (y_1\,y_2\,y_3)^{D/2-2}\;\Theta(y_1)\,\Theta(y_2)\,\Theta(y_3)\,\delta(1-y_1-y_2-y_3)\;.\end{aligned} \tag{98}$$

Now we are in the position to calculate the full real radiation contribution. The matrix element (for one quark flavour with charge q_f) in the variables defined above, where p_3 is the gluon, is given by

$$|\mathcal{M}|^2_{\mathrm{real}} = C_F e^2 q_f^2 g_s^2\,8\,(1-\epsilon)\left\{\frac{2}{y_2y_3}+\frac{-2+(1-\epsilon)y_3}{y_2}+\frac{-2+(1-\epsilon)y_2}{y_3}-2\epsilon\right\}\;. \tag{99}$$

In our variables, soft singularities mean $p_3 \to 0$ and therefore both y_2 and $y_3 \to 0$, while $p_3 \parallel p_1$ means $y_2 \to 0$ and $p_3 \parallel p_2$ means $y_3 \to 0$. Combined with the factors $(y_2\,y_3)^{D/2-2}$ from the phase space it is clear that the first term in the bracket of Eq. (99) will lead to a $1/\epsilon^2$ pole, coming from the region in phase space where soft and collinear limits coincide. The integrals can be expressed in terms of Euler Beta-functions and lead to the result quoted in Eq. (86).

4.2 Soft gluon emission

Soft gluon emission is very important in QCD. In contrast to the collinear case, soft gluons are insensitive to the spin of the partons. The only feature they are sensitive to is the colour charge.

To see this, consider the amplitude for the second row in Fig. 20, with momentum k and colour index a for the gluon, and momenta and colour indices p, i ($\bar{p}, j$) for the quark (antiquark). The amplitude for massless quarks is given by

$$\mathcal{M}^{a,\mu}_{ij} = t^a_{ij}\,g_s\,\mu^\epsilon\bar{u}(p)\;\not{\epsilon}(k)\frac{\not{p}+\not{k}}{(p+k)^2}\Gamma^\mu v(\bar{p}) - t^a_{ij}\,g_s\,\mu^\epsilon\bar{u}(p)\Gamma^\mu\frac{\not{\bar{p}}+\not{k}}{(\bar{p}+k)^2}\;\not{\epsilon}(k)v(\bar{p})\;, \tag{100}$$

where Γ^μ describes a general interaction vertex with the photon, in our case $\Gamma^\mu = \gamma^\mu$. Now we take the soft limit, which means that all components of k are much smaller than p and $\bar{p}$, thus neglecting factors of $\not{k}$ in the numerator and k^2 in the denominator. Using the Dirac equation leads to

$$\begin{aligned}\mathcal{M}^{a,\mu}_{ij,soft} &= g_s\,\mu^\epsilon\,t^a_{ij}\,\bar{u}(p)\,\Gamma^\mu\,v(\bar{p})\left(\frac{2\epsilon(k)\cdot p}{2p\cdot k}-\frac{2\epsilon(k)\cdot\bar{p}}{2\bar{p}\cdot k}\right)\\ &\equiv g_s\,\mu^\epsilon\,J^{a,\nu}_{ij}(k)\epsilon_\nu(k)\,\mathcal{M}^\mu_{Born}\quad,\quad \mathcal{M}^\mu_{Born} = \bar{u}(p)\Gamma^\mu v(\bar{p})\;.\end{aligned} \tag{101}$$

The amplitude factorises completely into the product of the Born amplitude and the *soft gluon current*

$$J^{a,\nu}_{ij}(k) = \sum_{r=p,\bar{p}} T^a_{ij}\,\frac{r^\nu}{r\cdot k}\;, \tag{102}$$

In our example $T^a_{ij} = t^a_{ij}$ for $r = p$ and $T^a_{ij} = -t^a_{ij}$ for $r = \bar{p}$. This type of factorisation actually holds for

an arbitrary number of soft gluon emissions, and can be obtained using the "soft Feynman rules" shown in Fig. 22.

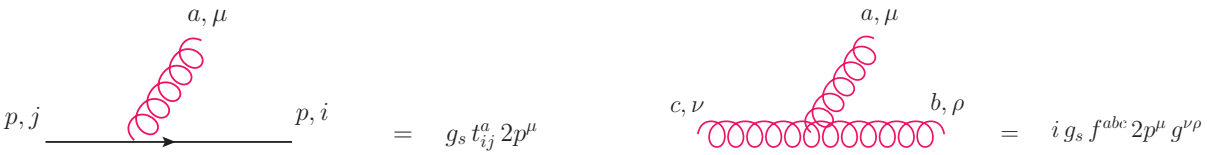

Fig. 22: The Feynman rules for gluon emission in the soft limit.

Following the standards set by Refs. [16,19], the soft gluon current is more conveniently expressed in terms of colour charge operators $\mathbf{T}_i$, where i now labels the *parton* i emitting a gluon (not its colour index).

The action of $\boldsymbol{T}_i$ onto the colour space is defined by

$$\langle a_1, \ldots, a_i, \ldots, a_m, a \,|\boldsymbol{T}_i|b_1, \ldots, b_i, \ldots, b_m\rangle = \delta_{a_1 b_1} \ldots . T^a_{a_i b_i} \ldots \delta_{a_m b_m} \quad , \tag{103}$$

where $T^a_{kl} \equiv t^a_{kl}$ ($SU(3)$ generator in the fundamental representation) if the emitting particle i is a quark. In the case of an emitting antiquark $T^a_{kl} \equiv \bar{t}^a_{kl} = -t^a_{lk}$. If the emitting particle i is a gluon, $T^a_{bc} \equiv -if_{abc}$ ($SU(3)$ generator in the adjoint representation).

Then we can write down the universal behaviour of the matrix element $\mathcal{M}(k, p_1, \ldots, p_m)$ in the limit where the momentum k of the gluon becomes soft. Denoting by a and $\varepsilon^\mu(k)$ the colour and the polarisation vector of the soft gluon, the matrix element fulfils the following factorisation formula:

$$\mathcal{M}^a(k, p_1, \ldots, p_m) \simeq g_s \, \mu^\epsilon \varepsilon^\mu(k) \, J^a_\mu(k) \, \mathcal{M}(p_1, \ldots, p_m) \, , \tag{104}$$

where $\mathcal{M}^a(p_1, \ldots, p_m)$ is obtained from the original matrix element by removing the soft gluon k. The factor $\boldsymbol{J}_\mu(k)$ is the soft-gluon current

$$\boldsymbol{J}^\mu(k) = \sum_{i=1}^{m} \boldsymbol{T}_i \, \frac{p_i^\mu}{p_i \cdot k} \, , \tag{105}$$

which depends on the momenta and colour charges of the hard partons in the matrix element on the right-hand side of Eq. (104). The symbol '$\simeq$' means that on the right-hand side we have neglected contributions that are less singular than $1/|k|$ in the soft limit $k \to 0$.

Squaring Eq. (104) and summing over the gluon polarisations leads to the *universal soft-gluon factorisation formula* at $\mathcal{O}(\alpha_s)$ for the squared amplitude [16]

$$|\mathcal{M}(k, p_1, \ldots, p_m)|^2 \simeq -g_s^2 \, \mu^{2\epsilon} \, 2 \sum_{i,j=1}^{m} S_{ij}(k) \, |\mathcal{M}_{(i,j)}(p_1, \ldots, p_m)|^2 \quad , \tag{106}$$

where the factor

$$S_{ij}(p_s) = \frac{p_i \cdot p_j}{2 \, (p_i \cdot p_s) \, (p_j \cdot p_s)} = \frac{s_{ij}}{s_{is} \, s_{js}} \tag{107}$$

is called the *Eikonal factor*. It can be generalised to the emission of n soft gluons and plays an important role in resummation.

The colour correlations produced by the emission of a soft gluon are taken into account by the square of the colour-correlated amplitude $|\mathcal{M}_{(i,j)}|^2$, given by

$$\begin{aligned}|\mathcal{M}_{(i,j)}(p_1,\ldots,p_m)|^2 &\equiv \langle\, \mathcal{M}(p_1,\ldots,p_m)\,|\,\boldsymbol{T}_i\cdot\boldsymbol{T}_j\,|\,\mathcal{M}(p_1,\ldots,p_m)\rangle \\ &= \left(\mathcal{M}_{c_1..b_i..b_j..c_m}(p_1,\ldots,p_m)\right)^*\; T^a_{b_i d_i}\,T^a_{b_j d_j}\;\mathcal{M}_{c_1..d_i..d_j..c_m}(p_1,\ldots,p_m)\;.\end{aligned}$$

The angular brackets in the second line denote a basis in colour space.

4.3 Collinear singularities

Let us come back to the amplitude for the real radiation given in Eq. (100). In a frame where $p = E_p(1,\vec{0}^{(D-2)},1)$ and $k = k_0(1,\vec{0}^{(D-3)}\sin\theta,\cos\theta)$, the denominator $(p+k)^2$ is given by

$$(p+k)^2 = 2k_0E_p\,(1-\cos\theta) \quad \to 0 \quad \text{for} \begin{cases} k_0\to 0 & \text{(soft)} \\ \theta\to 0 & \text{(collinear)}\end{cases} \tag{108}$$

Note that if the quark line was massive, $p^2 = m^2$, we would have

$$(p+k)^2 - m^2 = 2k_0E_p\,(1-\beta\cos\theta)\,, \quad \beta = \sqrt{1-m^2/E_p^2}$$

and thus the collinear singularity would be absent. This is why collinear singularities are sometimes also called *mass singularities*, since the propagator can only develop a collinear divergence if the splitting partons are massless, while the soft singularity is present irrespective of the mass of the quark radiating a gluon.

The important point to remember is that in the collinear limit, we also have a form of factorisation, shown schematically in Fig. 23.

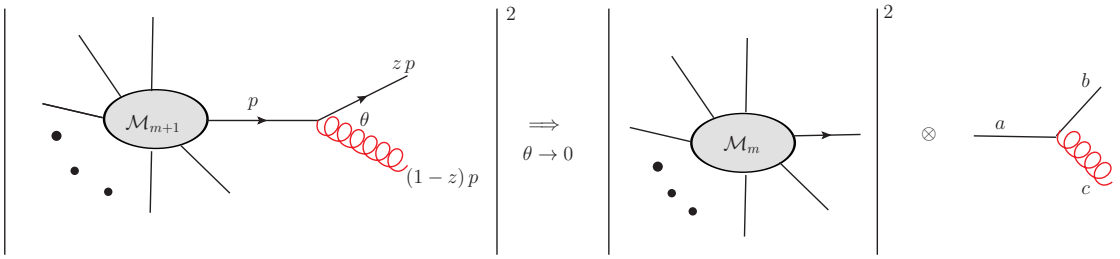

Fig. 23: Factorisation in the collinear limit.

The universal factorisation behaviour can be described as

$$|\mathcal{M}_{m+1}|^2\,\mathrm{d}\Phi_{m+1} \to |\mathcal{M}_m|^2\mathrm{d}\Phi_m\,\frac{\alpha_s}{2\pi}\,\frac{\mathrm{d}k_\perp^2}{k_\perp^2}\,\frac{\mathrm{d}\phi}{2\pi}\,\mathrm{d}z\,P_{a\to bc}(z)\;, \tag{109}$$

where we have used the so-called *Sudakov parametrisation*:

$$k^\mu = (1-z)\,p^\mu + \beta\,n^\mu + k_\perp^\mu\,, \tag{110}$$
$$k^+ = k\cdot n = (1-z)\,p\cdot n\,, \quad k^- = k\cdot p = \frac{k_\perp^2}{2(1-z)}\,,$$

with n^μ being a light-like vector satisfying $p\cdot n \neq 0$ and $k_\perp \cdot n = 0$, and β being determined by the requirement that k must be light-like:

$$k^2 = 0 = 2(1-z)\,\beta\,p\cdot n - k_\perp^2 \Rightarrow \beta = \frac{k_\perp^2}{2\,p\cdot n\,(1-z)}\,. \tag{111}$$

The function $P_{a\to bc}(z)$ is the so-called *Altarelli–Parisi splitting function*, describing the splitting of parton a into partons b and c, and z is the momentum fraction of the original parton a taken away by parton b after emission of c. For example, consider collinear gluon emission off a quark:

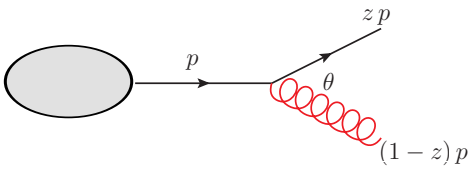

Fig. 24: Gluon emission leading to $P_{q\to qg}(z)$.

The corresponding Altarelli-Parisi splitting function for $z < 1$ is given by

$$P_{q\to qg}(z) = C_F\,\frac{1+z^2}{1-z}\,, \tag{112}$$

and is often just denoted as $P_{qq}(z)$. The other possible splitting functions have the following form:

$$P_{q\to gq}(z) = C_F\,\frac{1+(1-z)^2}{z}\,, \quad P_{g\to q\bar{q}}(z) = T_R\,\left(z^2+(1-z)^2\right)\,,$$
$$P_{g\to gg}(z) = C_A\,\left(z\,(1-z) + \frac{z}{1-z} + \frac{1-z}{z}\right)\,. \tag{113}$$

We will come back to them later when we discuss parton distribution functions.

4.3.1 Jet cross sections and jet algorithms

Jets can be pictured as clusters of particles which are close to each other in phase space, resp. in the detector.

In Fig. 25 (left), a typical composition of the different types of particles making up jets, in terms of the fraction of the total jet energy carried by the particles, is shown for a simulated 2-jet event at the LHC. These jets are primarily composed of charged and neutral pions. Further, baryons and other types of mesons contribute a moderate fraction of the total jet energy, and small energy fractions of electrons and muons are also present, originating from heavy hadron decays. Until today, jets have been measured over a very large energy range at different colliders, see Fig. 25 (right).

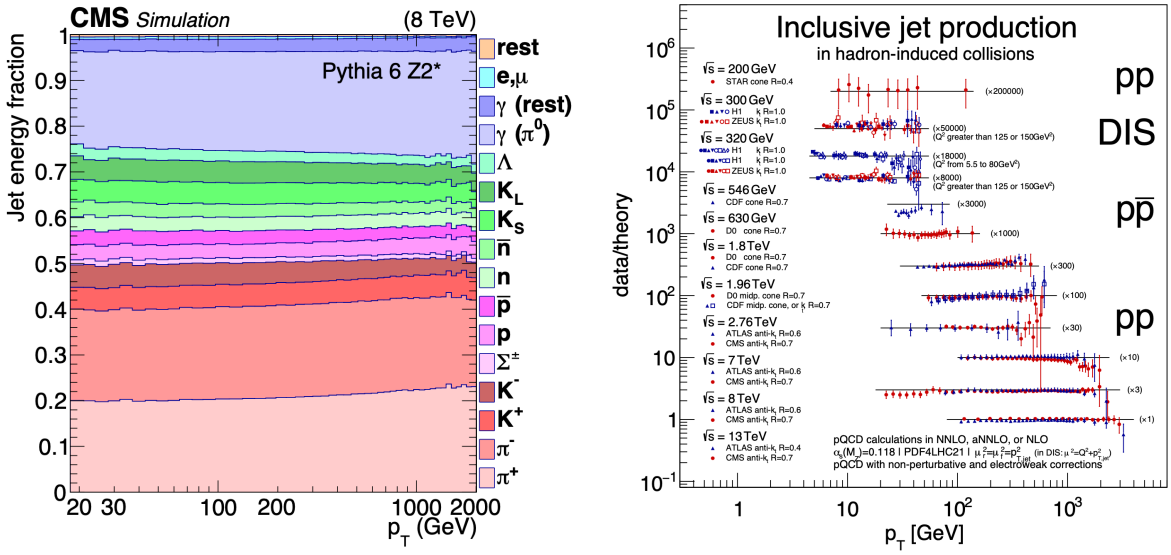

Fig. 25: Left: The fraction of the total jet energy carried by different types of particles forming jets (simulated LHC dijet events). Right: Data over theory predictions for inclusive jet production at different experiments and center-of-mass energies. *Figures from Ref. [48], B. Malaescu et al., D. Britzger et al.*

Sterman–Weinberg jet definition

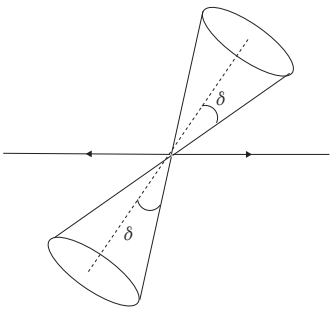

Fig. 26: Two jet cones according to the definition of Sterman and Weinberg.

Historically, one of the first suggestions to define jet cross sections was by Sterman and Weinberg [73]. In their definition, a final state is classified as two-jet-like if all but a fraction ε of the total available energy E is contained in two cones of opening angle δ. The two-jet cross section is then obtained by integrating the matrix elements for the various quark and gluon final states over the appropriate region of phase space determined by ε and δ.

Of course the two-jet cross section depends on the values for ε and δ. If they are very large, even extra radiation at a relatively large angle $\theta < \delta$ will be "clustered" into the jet cone and almost all events will be classified as 2-jet events. If they are very small, the 2-jet cross section starts to diverge, because "one parton" is not an observable, it cannot be distingushed from "one parton plus soft and/or collinear radiation".

More modern jet algorithms

The Sterman–Weinberg jet definition based on cones is not very practical to analyse multijet final states. A better alternative is for example the following:

1. starting from n particles, for all pairs i and j calculate $(p_i + p_j)^2$.
2. If $\min(p_i + p_j)^2 < y_{\rm cut}\, Q^2$ then define a new "pseudo-particle" $p_J = p_i + p_j$, which decreases $n \to n - 1$. Q is the center-of-mass energy in e^+e^- collisions, or a typical hard scattering energy in hadronic collisions, and $y_{\rm cut}$ is the jet resolution parameter.
3. if $n = 1$, stop, else repeat the step above.

After this algorithm, all partons are clustered into jets. This simple algorithm is sometimes called JADE-algorithm because it has been used first at the JADE experiment at PETRA (DESY). With this definition one finds at $\mathcal{O}(\alpha_s)$:

$$\sigma^{2\,jet} = \sigma_0 \left(1 - C_F \frac{\alpha_s}{\pi} \left[\ln^2 y_{\rm cut} + \frac{3}{2} \ln y_{\rm cut} + \text{ finite}\right]\right) . \tag{114}$$

Algorithms which are particularly useful for hadronic initial states are e.g. the so-called Durham-k_T algorithm [10] or the anti-k_T algorithm [14]. Both algorithms are based on a distance measure

$$d_{ij} = \min(p_{T,i}^{2p}, p_{T,j}^{2p}) \frac{\Delta R_{ij}^2}{R^2} , \tag{115}$$

where R is a radius parameter, $\Delta R_{ij}^2 = \Delta y_{ij}^2 + \Delta\phi_{ij}^2$ is the distance in rapidity and azimuthal angle between particles i and j, and the parameter p is 1 for the k_T algorithm, 0 for the Cambridge–Aachen [33] algorithm and -1 for the anti-k_T algorithm. The distance d_{ij} is calculated for all combinations of pairs of particles. The pair with the lowest d_{ij} is replaced by a pseudo-particle whose four-momentum is given by the sum of the four-momenta of particles i and j. Summing the 4-momenta to form the pseudo-particle is also called "E-recombination scheme". Note that the combined 4-momentum is not light-like anymore. The clustering procedure is repeated as long as pairs with invariant mass fraction below a predefined resolution parameter $y_{\rm cut}$ are found. Once the clustering is terminated, the remaining (pseudo-)particles are the jets. Figures 27 and 28 illustrate how the jet areas depend on the jet algorithm and the jet radius R.

It is evident that a large value of $y_{\rm cut}$ will ultimately result in the clustering all particles into only two jets, while higher jet multiplicities will become more and more frequent as $y_{\rm cut}$ is lowered. In experimental jet measurements, one therefore studies the jet rates (n-jet cross sections normalised to the total hadronic cross section) as function of the jet resolution parameter $y_{\rm cut}$. Figure 29 (left) shows the jet rates as a function of $y_{\rm cut}$, compared to ALEPH data. Figure 29 (right) shows corrections up to NNLO to the 3-jet rate as a function of $y_{\rm cut}$. Note that in this figure, for small values of $y_{\rm cut}$, the 3-jet rate at LO diverges (green band) because it shows a partonic calculation: only three partons are present at LO and therefore there is no room for extra radiation. As an isolated parton is not an observable, the cross section diverges in this limit. At higher orders, this situation is somewhat cured by extra radiation being allowed, however resummation or parton showering would be needed to achieve a better description of the very low $y_{\rm cut}$ region.

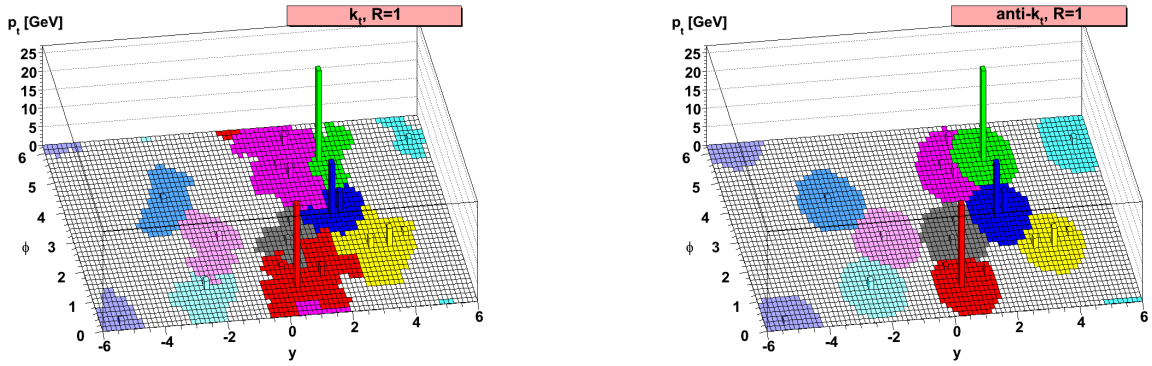

Fig. 27: Jet areas as a result of (a) the Durham-k_T algorithm, (b) the anti-k_T algorithm. Figures from Ref. [14].

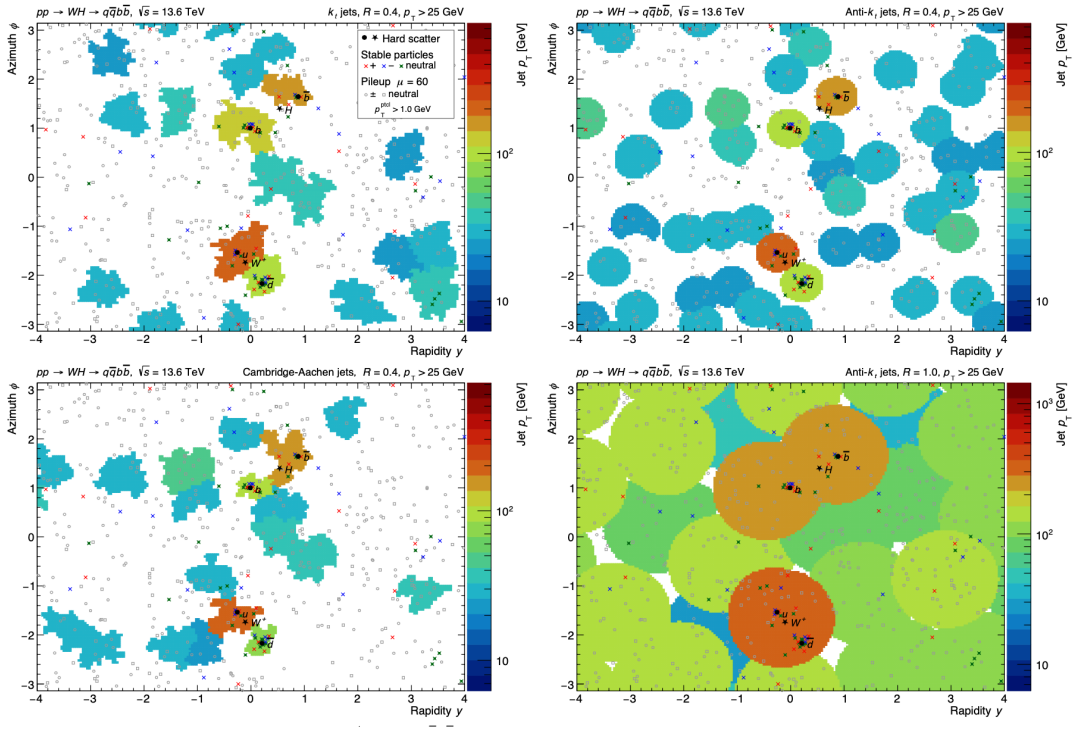

Fig. 28: Jet areas as a result of different jet algorithms and jet radii R. Figure from Ref. [48].

At the LHC, the most commonly used jet algorithm is the *anti-k_T algorithm* [14]. Of course it is very important that jet algorithms are infrared safe. The standard tool for jet identification in simulation programs is `fastjet`, see `http://fastjet.fr/`. More details about jet algorithms can be found in Ref. [71].

4.3.2 Jet substructure

The investigation of jet substructure is relatively recent and has developed into an essential tool for the LHC physics program. Information about the jet substructure is very useful to disentangle different kinds of jets, such as separating quark-initiated jets from gluon-initiated jets or isolating jets from boosted W, Z, H- or top-quark-decays from the background of quark and gluon-initiated jets.

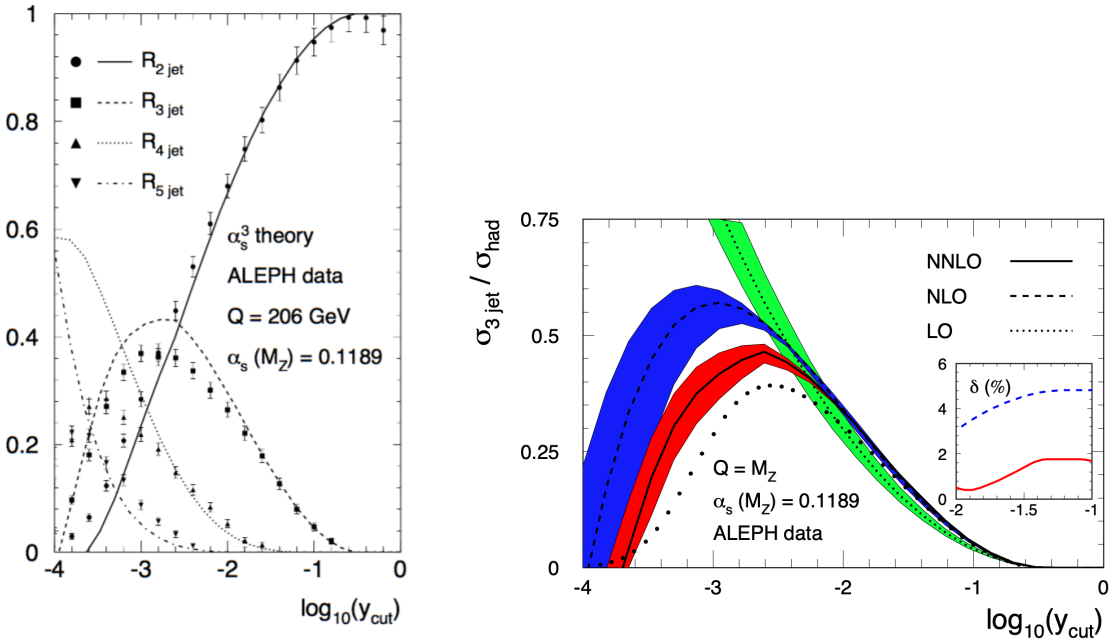

Fig. 29: Left: Jet rates as a function of the jet resolution parameter y_{cut} [51]. Right: higher-order corrections to the 3-jet rate [41].

Jet substructure tools aim to get information about the internal kinematic properties of a high-p_T jet. Important quantities in this context are the invariant jet mass M^2_{jet}, defined as

$$M^2_{\text{jet}} = \left(\sum_{i \in \text{jet}} p_i \right)^2 , \tag{116}$$

where the p_i denote the 4-momenta of the jet constituents, and the generalised jet angularities λ_β, defined as [64]

$$\lambda_\beta = \sum_{i \in \text{jet}} z_i \left(\frac{\Delta R_{i,\text{jet}}}{R} \right)^\beta , \tag{117}$$

where z_i is the jet transverse momentum fraction carried by the constituent i and $\Delta R_{i,\text{jet}}$ is its distance to the jet axis in the $(y - \phi)$–plane:

$$z_i = \frac{p_{t,i}}{\sum_{j \in \text{jet}} p_{t,j}} \qquad \text{and} \qquad \Delta R^2_{i,\text{jet}} = (y_i - y_{\text{jet}})^2 + (\phi_i - \phi_{\text{jet}})^2 . \tag{118}$$

Gluon-initiated jets in general have larger angularities than quark-initiated jets. A large variety of methods for jet substructure have been proposed over the last ten years, for more details we refer to Ref. [64].

While the jet mass and other jet substructure indicators provide a solid baseline, modern jet substructure classifiers make use of machine learning techniques to maximally discriminate between different possible jet origin interpretations.

4.3.3 *Event shapes*

Of course, jets are not the only observables one can define based on hadronic tracks in the detector. Other very useful observables are so-called *event-shape* observables, for example *thrust*, which describes how "pencil-like" an event looks. Thrust T is defined by

$$T = \max_{\vec{n}} \frac{\sum_{i=1}^{m} |\vec{p}_i \cdot \vec{n}|}{\sum_{i=1}^{m} |\vec{p}_i|} , \tag{119}$$

where $\vec{n}$ is a three-vector (the direction of the thrust axis) such that T is maximal. The particle three-momenta $\vec{p}_i$ are defined in the centre-of-mass frame. Therefore, the above definition only holds for lepton colliders where the partonic centre-of-mass energy is fixed. At hadron colliders, the definition of event shapes such as thrust is still possible, but in this case it is based on transverse momenta. T is an example of a measurement function $J(p_1, \ldots, p_m)$. It is infrared safe because neither $p_j \to 0$, nor replacing p_i with $zp_i + (1-z)p_i$ change T. Figure 30 shows the collinear and soft regions in a Dalitz-plot, where x_i

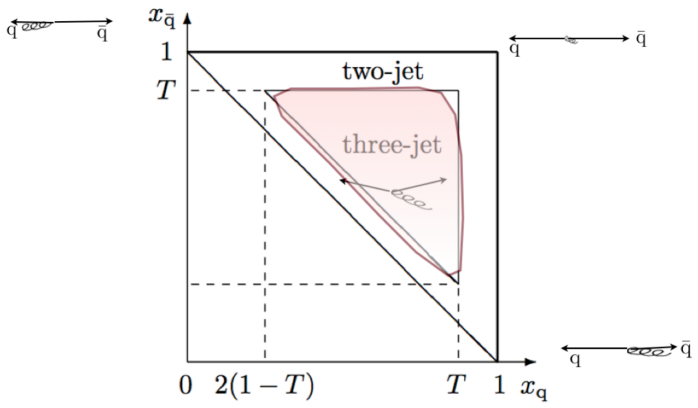

Fig. 30: Dalitz-plot showing the allowed 2-jet and 3-jet regions and thrust values. Figure from Ref. [30].

denote the energy fractions, defined by

$$x_q = 2\frac{E_q}{\sqrt{s}} , \quad x_{\bar{q}} = 2\frac{E_{\bar{q}}}{\sqrt{s}} , \quad x_g = 2\frac{E_g}{\sqrt{s}} , \quad x_q + x_{\bar{q}} + x_g = 2 . \tag{120}$$

At leading order it is possible to perform the phase space integrations analytically, to obtain

$$\frac{1}{\sigma}\frac{\mathrm{d}\sigma}{\mathrm{d}T} = C_F \frac{\alpha_s}{2\pi}\left[\frac{2(3T^2-3T+2)}{T(1-T)}\ln\left(\frac{2T-1}{1-T}\right) - 3(3T-2)\frac{2-T}{1-T}\right] . \tag{121}$$

We see that the perturbative prediction for the thrust distribution becomes singular as $T \to 1$. In addition to the factor of $1-T$ in the denominator, there is also a logarithmic divergence $\sim \ln(1-T)$. The latter is characteristic for event shape distributions. For an event shape Y with $Y \to 0$ in the two-jet limit (so for example $Y = 1-T$), the behaviour at n-th order in perturbation theory is [17] $\frac{1}{\sigma}\frac{d\sigma^{(n)}}{dY} \simeq \alpha_s^n \frac{1}{Y}\ln^{2n-1}(\frac{1}{Y})$. These logarithms spoil the convergence of the perturbative series and should be "resummed" if we want to make reliable prediction near the phase-space region where $Y \to 0$. Summing the leading logarithms to all orders leads to an exponential function providing a "damping factor", the so-called Sudakov-factor.

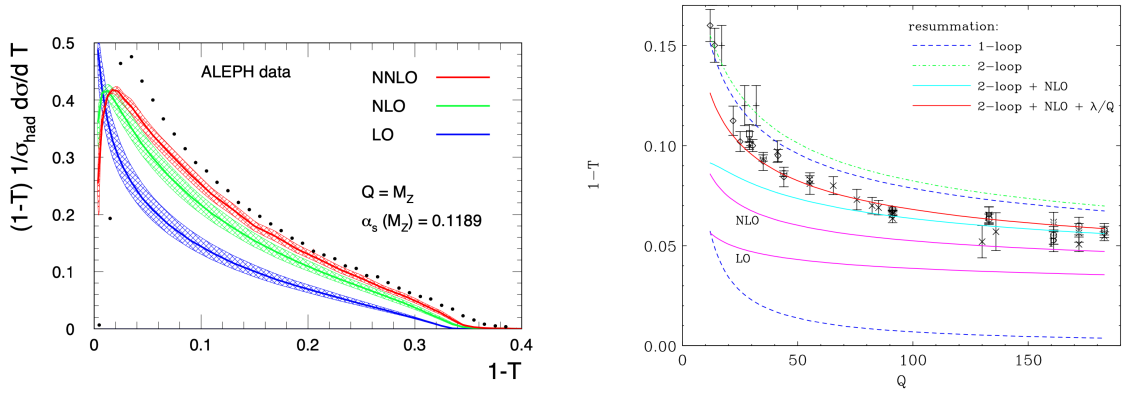

Fig. 31: Left: The thrust distribution up to NNLO in QCD, compared to ALEPH data. Figure from Ref. [40]. Right: The thrust distribution up to NLO in QCD and including resummation and power corrections, compared to data. Figure from Ref. [39].

Figure 31 (left) shows the thrust distribution up to NNLO precision in QCD. This is an observable where both resummation and power corrections $\sim \lambda/Q$ need to be included to describe the data well over the whole kinematic range, as can be seen from Fig. 31 (right).

5 PDFs and parton evolution

5.1 Deeply inelastic scattering

In the discussion of the cancellation of IR singularities we have only considered leptons in the initial state (e^+e^- annihilation). Now we consider the case where we have an electron–proton collider, like for example HERA, which operated at DESY until 2007 and offered unique opportunities to study the proton structure. We consider the scattering of electrons off the proton by photon exchange, as depicted in Fig. 32, in a kinematic regime where the squared momentum transfer Q^2 is large compared to the proton mass squared ($M \sim 1\,\text{GeV}$), so we consider deeply inelastic scattering (DIS), $e(k)+p(P) \to e(k')+X$, where P is the momentum of the proton. The relations between the involved momenta and some useful

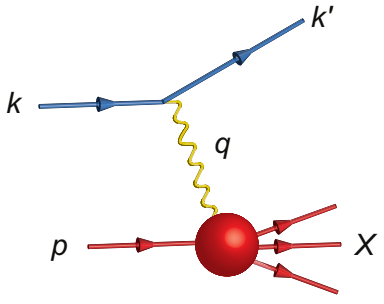

Fig. 32: Deeply inelastic scattering. Figure from Ref. [2].

kinematic variables are

$$s = (P+k)^2 \quad [\text{cms energy}]^2$$

$$
\begin{aligned}
q^\mu &= k^\mu - k'^\mu \ \text{[momentum transfer]} \\
Q^2 &= -q^2 = 2MExy \\
x &= \frac{Q^2}{2P\cdot q} \ \text{[scaling variable]} \\
y &= \frac{P\cdot q}{P\cdot k} = 1 - \frac{E'}{E} \ \text{[relative energy loss]} \, .
\end{aligned} \tag{122}
$$

The cross section can be written as

$$
\int \mathrm{d}\sigma = \sum_X \frac{1}{4ME} \int \mathrm{d}\Phi \, \frac{1}{4} \sum_{\text{spins}} |\mathcal{M}|^2 \, . \tag{123}
$$

We can factorise the squared matrix element into a leptonic tensor $L^{\mu\nu}$ and a hadronic tensor $H_{\mu\nu}$, and also factorise the phase space,

$$
\mathrm{d}\Phi = \frac{\mathrm{d}^3k'}{(2\pi)^3 2E'} \, \mathrm{d}\Phi_X \, , \quad \frac{1}{4} \sum_{\text{spins}} |\mathcal{M}|^2 = \frac{e^4}{Q^4} L^{\mu\nu} H_{\mu\nu} \, . \tag{124}
$$

Then the hadronic part of the cross section can be described by the dimensionless Lorentz tensor $W_{\mu\nu} = \frac{1}{8\pi} \sum_X \int \mathrm{d}\Phi_X H_{\mu\nu}$. As it depends only on two momenta P^μ and q^μ, the most general gauge- and Lorentz-invariant expression must be of the form

$$
\begin{aligned}
W_{\mu\nu}(P,q) = &\left(-g_{\mu\nu} + \frac{q_\mu q_\nu}{q^2} \right) W_1(x, Q^2) \\
&+ \left(P_\mu - q_\mu \frac{P\cdot q}{q^2} \right) \left(P_\nu - q_\nu \frac{P\cdot q}{q^2} \right) \frac{W_2(x,Q^2)}{P\cdot q} \, ,
\end{aligned} \tag{125}
$$

where the structure functions $W_i(x, Q^2)$ are dimensionless functions of the scaling variable x and the momentum transfer Q^2.

For the leptonic part we use the relations $E' = (1-y)E$, $\cos\theta = 1 - \frac{xyM}{(1-y)E}$ to change variables to x and the relative energy loss y,

$$
\frac{\mathrm{d}^3k'}{(2\pi)^3 2E'} = \frac{\mathrm{d}\phi}{2\pi} \frac{E'}{8\pi^2} \, \mathrm{d}E' \, \mathrm{d}\cos\theta = \frac{\mathrm{d}\phi}{2\pi} \frac{yME}{8\pi^2} \, \mathrm{d}y \, \mathrm{d}x \, ,
$$

and compute the trace $L^{\mu\nu} = \frac{1}{2} Tr[\not{k}\gamma^\mu \not{k}'\gamma^\nu] = k^\mu k'^\nu + k^\nu k'^\mu - g^{\mu\nu} k\cdot k'$. Then the differential cross section in x and y is obtained from Eq. (123) as

$$
\frac{\mathrm{d}^2\sigma}{\mathrm{d}x \, \mathrm{d}y} = \frac{4\pi\alpha^2}{y\,Q^2} \left[y^2 W_1(x,Q^2) + \left(\frac{1-y}{x} - xy\frac{M^2}{Q^2} \right) W_2(x,Q^2) \right] \, .
$$

In the *scaling limit*, defined by $Q^2 \to \infty$ with x fixed, we use $W_1 \to -F_1, W_2 \to F_2$, neglect the term $\sim M^2/Q^2$ and obtain

$$
\frac{\mathrm{d}^2\sigma}{\mathrm{d}x \, \mathrm{d}y} = \frac{4\pi\alpha^2}{y\,Q^2} \left[\big(1 + (1-y)^2\big) F_1 + \frac{1-y}{x} \big(F_2 - 2xF_1 \big) \right] \, . \tag{126}
$$

The functions F_1 and F_2 are called *structure functions*, where the combination $F_L = F_2 - 2xF_1$ is also called the longitudinal structure function because it is related to the absorption of a longitudinally polarised virtual photon. They were first measured by the SLAC–MIT experiment (USA) in 1970, and have been measured very accurately at the HERA collider. A very interesting feature is the fact that, in the scaling limit, we observe that $2xF_1 \to F_2$ and that F_2 becomes independent of Q^2, $F_2(x, Q^2) \to F_2(x)$, a feature which is often called *Bjorken scaling*. Furthermore, the *Callan–Gross* relation $F_2(x) = 2x\, F_1(x)$ can be derived from first principles under the assumption that the photon scatters off point-like spin-1/2 particles. These observations were very important to establish the quark model. How the scaling looks in experiment is shown in Fig. 33, where we see that scaling violations are present, increasing at small x. This can be explained by considering corrections to the naïve quark model.

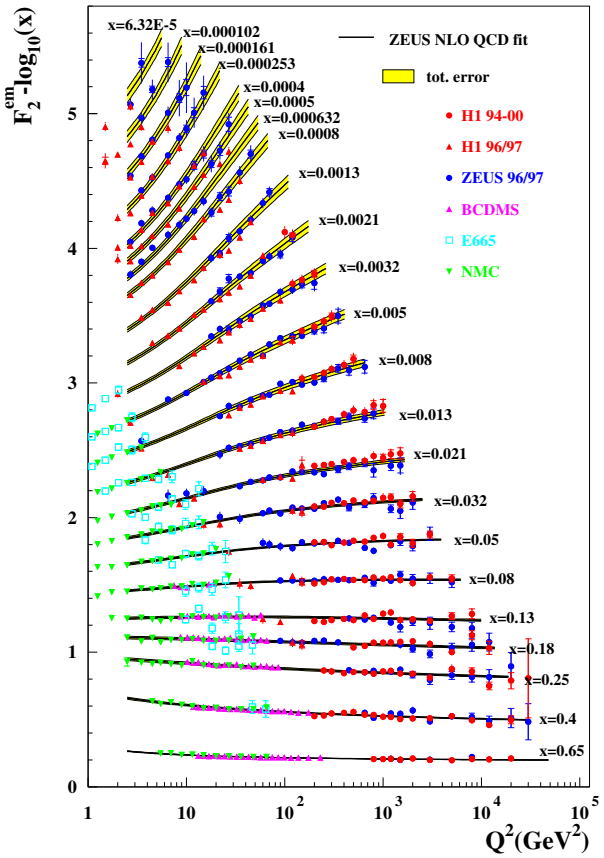

Fig. 33: The structure function F_2 for different values of Q^2. Figure from Ref. [59].

5.2 Proton structure in the parton model

Now let us assume the proton consists of free quarks and the lepton exchanges a hard virtual photon with one of those quarks. The struck quark carries a momentum p^μ, which is a fraction of the proton momentum, $p^\mu = \xi P^\mu$, so we consider the process $e(k) + q(p) \to e(k') + q(p')$. The corresponding

cross section is

$$\hat{\sigma} = \frac{1}{2\hat{s}} \int \mathrm{d}\Phi_2 \, \frac{1}{4} \sum_{\text{spins}} |\mathcal{M}|^2 \, . \tag{127}$$

with $\hat{s} = (p+k)^2$. The "hat" indicates that we consider the partonic cross section. The squared matrix element is proportional to the product of the leptonic tensor $L^{\mu\nu}$ and a quark tensor $Q_{\mu\nu}$, with $Q_{\mu\nu} = \frac{1}{2} Tr[\not{p}\gamma^\mu \not{p}'\gamma^\nu] = p^\mu p'^\nu + p^\nu p'^\mu - g^{\mu\nu} p \cdot p'$, leading to $L^{\mu\nu} Q_{\mu\nu} = 2(\hat{s}^2 + \hat{u}^2)$, where $\hat{u} = (p-k')^2 = -2p \cdot k'$. As $y = Q^2/\hat{s}$ we can derive, using $\hat{u}^2 = (1-y)^2 \hat{s}^2$,

$$\frac{1}{4} \sum_{\text{spins}} |\mathcal{M}|^2 = \frac{e_q^2 e^4}{Q^4} L^{\mu\nu} Q_{\mu\nu} = 2 e_q^2 e^4 \frac{\hat{s}^2}{Q^4} \left(1 + (1-y)^2\right) \, . \tag{128}$$

Using $p'^2 = 2p \cdot q - Q^2 = Q^2(\xi/x - 1)$, the two-particle phase space (in 4 dimensions) can be written as

$$\mathrm{d}\Phi_2 = \frac{\mathrm{d}^3 k'}{(2\pi)^3 2E'} \frac{\mathrm{d}^4 p'}{(2\pi)^3} \, \delta\left(p'^2\right) (2\pi)^4 \, \delta^{(4)}(k + p - k' - p') = \frac{\mathrm{d}\phi}{(4\pi)^2} \, \mathrm{d}y \, \mathrm{d}x \, \delta(\xi - x) \, . \tag{129}$$

The differential cross section in x and y for one quark flavour is then given by

$$\frac{\mathrm{d}^2 \hat{\sigma}}{\mathrm{d}x \, \mathrm{d}y} = \frac{4\pi\alpha^2}{yQ^2} \left[1 + (1-y)^2\right] \frac{1}{2} e_q^2 \delta(\xi - x) \, . \tag{130}$$

Comparing Eqs. (126) and (130), we find the parton model predictions

$$\hat{F}_1(x) \propto e_q^2 \delta(\xi - x) \, , \qquad F_2 - 2xF_1 = 0 \, . \tag{131}$$

Therefore we found that the *Callan–Gross* relations follow directly from the assumption that a quark contained in the proton is responsible for the hard scattering. Thus the structure functions probe the quark constituents of the proton with $\xi = x$. However, this prediction cannot be the end of the story because experimentally, we observe that F_2 does depend on Q^2, as can be seen from Fig. 33, even though the dependence is not strong.

To see how the Q^2 dependence comes in, let us define the following:

$f_i(\xi)\mathrm{d}\xi$ is the probability to find a parton $(q, \bar{q}, g)$ with flavour i in the proton, carrying a momentum fraction of the proton between ξ and $\xi + \delta\xi$.

The function $f_i(\xi)$ is called *parton distribution function (PDF)*.

Using the relations $\mathrm{d}y = \mathrm{d}Q^2/\hat{s}$ and $\delta(\xi - x) = \frac{1}{\xi}\delta\left(1 - \frac{x}{\xi}\right)$, we can write the full cross section as a combination of the PDF and the partonic cross section (130),

$$\frac{\mathrm{d}^2 \sigma}{\mathrm{d}x \, \mathrm{d}Q^2} = \int_x^1 \frac{\mathrm{d}\xi}{\xi} \sum_i f_i(\xi) \frac{\mathrm{d}^2 \hat{\sigma}}{\mathrm{d}x \, \mathrm{d}Q^2} \left(\frac{x}{\xi}, Q^2\right) \, . \tag{132}$$

This means that the cross section is a convolution of a long-distance component, the parton distribution function $f_i(\xi)$ for a parton of type i, and a short-distance component, the partonic hard scattering cross

section $\hat{\sigma}$. This *factorisation* (up to power corrections), mentioned already in Section 2.1, can be proven rigorously in DIS using operator product expansion, and less rigorously in hadron–hadron collisions.

According to eqs. (126) and (132), we find in the naïve parton model

$$F_2(x) = 2xF_1(x) = \sum_i \int_0^1 \mathrm{d}\xi\, f_i(\xi)\, x\, e_{q_i}^2\, \delta(x-\xi) = x \sum_i e_{q_i}^2\, f_i(x)\ . \tag{133}$$

For a proton probed at a scale Q, we expect it to consist mostly of uud. Writing $f_i(x) = u(x), d(x)$ etc. for $i = u, d, \ldots$ we have in the naïve parton model

$$F_2^{\text{proton}}(x) = x\Big[\frac{4}{9}\big(u(x)+\bar{u}(x)\big) + \frac{1}{9}\big(d(x)+\bar{d}(x)\big)\Big]\ . \tag{134}$$

If we define the so-called "valence quarks" $u_v(x) u_v(x) d_v(x)$,

$$u(x) = u_v(x) + \bar{u}(x)\ ,\ d(x) = d_v(x) + \bar{d}(x)\ ,\ s(x) = \bar{s}(x)\ ,$$

we expect the "sum rules"

$$\int_0^1 \mathrm{d}x\, u_v(x) = 2\ , \quad \int_0^1 \mathrm{d}x\, d_v(x) = 1\ , \quad \int_0^1 \mathrm{d}x\, (s(x)-\bar{s}(x)) = 0\ . \tag{135}$$

Figure 34 illustrates that, the smaller x and the larger Q^2, the more the "sea quarks" and gluons in the proton are probed. In fact, it turns out that $\sum_{i=q,\bar{q}} \int_0^1 \mathrm{d}x\, x f_{i/p}(x) \simeq 0.5$, so quarks carry only about half of the momentum of the proton. Therefore the other half is carried by gluons; the naïve parton model is clearly not sufficient to describe the proton.

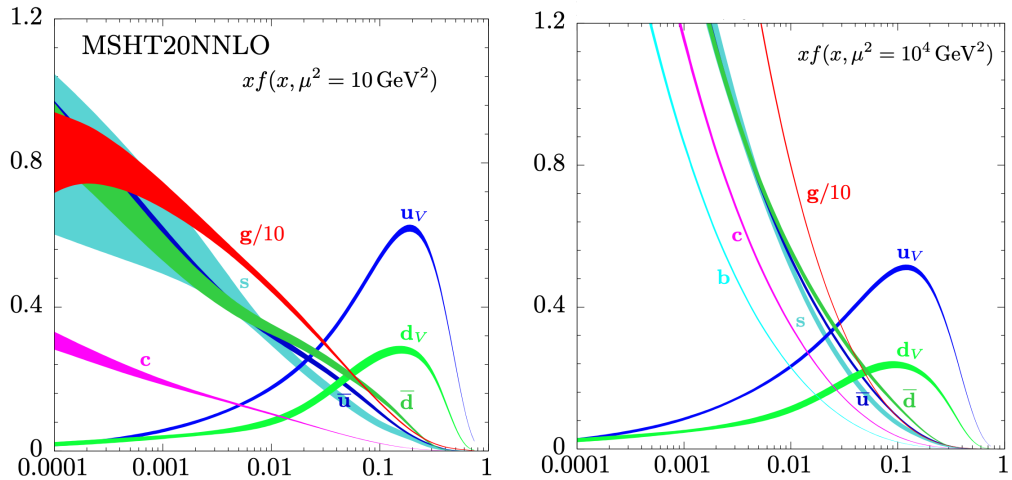

Fig. 34: Parton distribution functions in the proton as a function of x. Source: Particle Data Group, section *structure functions* [77].

5.3 Proton structure in perturbative QCD

Investigating what happens in the "QCD-improved" parton model, we will encounter again IR singularities and splitting functions. Let us denote the hard scattering cross section by σ_h. For final-state radiation, we found that the IR singularities due to soft and collinear configurations cancel against IR divergences in the virtual corrections for infrared safe quantities.

If there is a coloured parton in the *initial* state, the splitting may occur *before* the hard scattering, such that the momentum of the parton that enters the hard process is reduced to xp^μ.

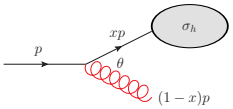

$$\mathrm{d}\sigma_{h+g}(p) \simeq \sigma_h(xp)\; 2C_F \frac{\alpha_s}{\pi}\frac{\mathrm{d}E}{E}\frac{\mathrm{d}\theta}{\theta} \to \sigma_h(xp)\, C_F \frac{\alpha_s}{\pi}\,\mathrm{d}x\,(1-x)^{-1-\epsilon}\,\mathrm{d}k_\perp^2\,(k_\perp^2)^{-1-\epsilon}\,.$$

Integrating over x and $k_\perp$ we find a soft divergence for $x \to 1$ and a collinear divergence for $k_\perp \to 0$. The corresponding $1/\epsilon$ poles multiply $\sigma_h(xp)$, while in the virtual correction the poles multiply $\sigma_h(p)$, irrespective whether the IR divergence is in the initial or final state:

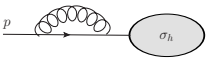

$$\mathrm{d}\sigma_V \simeq -\sigma_h(p)\, C_F \frac{\alpha_s}{\pi}\,\mathrm{d}x\,(1-x)^{-1-\epsilon}\,\mathrm{d}k_\perp^2\,(k_\perp^2)^{-1-\epsilon}\,.$$

Summing up the real and virtual corrections we remain with an uncanceled collinear singularity from the factor $(k_\perp^2)^{-1-\epsilon}$,

$$\mathrm{d}(\sigma_{h+g}+\sigma_V) \simeq C_F\frac{\alpha_s}{\pi}\,\mathrm{d}k_\perp^2\,(k_\perp^2)^{-1-\epsilon}\mathrm{d}x\,\underbrace{(1-x)^{-1-\epsilon}[\sigma_h(xp)-\sigma_h(p)]}_{\text{finite}}\,, \tag{136}$$

Note that the soft singularity for $x \to 1$ is regulated in the sum of real and virtual parts. The uncanceled collinear singularity in the initial state however remains. Fortunately its form is universal, i.e. independent of the details of the hard scattering process, only dependent on the type of parton splittings. Therefore we can also eliminate it in a universal way: It is absorbed into "bare" parton densities, $f_i^{(0)}(x)$, such that the measured parton densities are the "renormalised" ones. This procedure is very similar to the renormalisation of UV divergences and introduces a scale μ_f, the *factorisation scale*, into the parton densities. Let us see how this works for the structure function F_2. We first consider the *partonic* structure functions $\hat{F}_{2,q}, \hat{F}_{2,g}$, where the subscript q indicates that a quark is coming out of the proton, analogous for a gluon g. Note that a gluon coming from the proton does not interact with a photon, therefore the gluonic contribution is zero at leading order, but it will appear at order α_s because the gluon can split into a $q\bar{q}$ pair and then one of the quarks interacts with the photon. Hence we have

$$\hat{F}_{2,q}(x) = \left.\frac{\mathrm{d}^2\hat{\sigma}}{\mathrm{d}x\,\mathrm{d}Q^2}\right|_{F_2} = e_q^2 x\left[\delta(1-x)+\frac{\alpha_s}{4\pi}\left(-\left(\frac{Q^2}{\mu^2}\right)^{-\epsilon}\frac{1}{\epsilon}\,P_{q\to qg}(x)+C_2^q(x)\right)\right], \tag{137}$$

$$\hat{F}_{2,g}(x) = \left.\frac{\mathrm{d}^2\hat{\sigma}}{\mathrm{d}x\,\mathrm{d}Q^2}\right|_{F_2} = \sum_q e_q^2 x\left[0+\frac{\alpha_s}{4\pi}\left(-\left(\frac{Q^2}{\mu^2}\right)^{-\epsilon}\frac{1}{\epsilon}\,P_{g\to q\bar{q}}(x)+C_2^g(x)\right)\right], \tag{138}$$

where $P_{j\to ik}(x)$ is the Altarelli–Parisi splitting function (regularised at $x=1$) which we already encoun-

tered when discussing collinear singularities. It denotes the probability that a parton j splits collinearly into partons i and k, with i carrying a momentum fraction x of the original parton j. Note that the type of parton k is fixed by i and j. Therefore i and j are sufficient to label the splitting functions. For the labelling different conventions are in use, they are summarised in Table 2. $C_2(x)$ is the remaining finite term, sometimes called coefficient function. The partonic function $\hat{F}_2$ is not measurable, only the proton structure function F_2 is physical. Therefore we have to form the convolution of the partonic part with the parton distribution functions.

$P_{ij}(x)$	$P_{j\to ik}(x)$	$P_{i/j}(x)$
$P_{qq}(x)$	$P_{q\to qg}(x)$	$P_{q/q}(x)$
$P_{gq}(x)$	$P_{q\to gq}(x)$	$P_{g/q}(x)$
$P_{qg}(x)$	$P_{g\to q\bar{q}}(x)$	$P_{q/g}(x)$
$P_{gg}(x)$	$P_{g\to gg}(x)$	$P_{g/g}(x)$

Table 2: Translation between different conventions for the labelling of the splitting functions, see also Fig. 35.

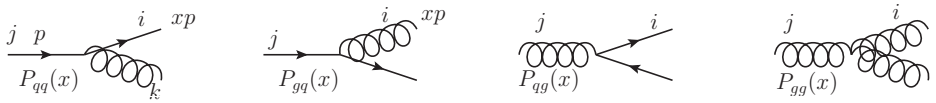

Fig. 35: Splitting functions with corresponding labelling.

$$F_{2,q}(x,Q^2) = x\sum_i e_{q_i}^2 \left[f_i^{(0)}(x) + \frac{\alpha_s}{2\pi}\int_x^1 \frac{\mathrm{d}\xi}{\xi} f_i^{(0)}(\xi)\left(-\left(\frac{Q^2}{\mu^2}\right)^{-\epsilon}\frac{1}{\epsilon}\,P_{q\to qg}\left(\frac{x}{\xi}\right) + C_2^q\left(\frac{x}{\xi}\right)\right)\right]. \tag{139}$$

Now we absorb the singularity into the parton distribution function by the definition

$$f_i(x,\mu_f^2) = f_i^{(0)}(x) + \frac{\alpha_s}{2\pi}\int_x^1 \frac{\mathrm{d}\xi}{\xi}\left\{ f_i^{(0)}(\xi)\left[-\frac{1}{\epsilon}\left(\frac{\mu_f^2}{\mu^2}\right)^{-\epsilon} P_{q\to qg}\left(\frac{x}{\xi}\right) + K_{qq}\right]\right\}, \tag{140}$$

where K_{qq} denotes finite terms depending on the regularisation scheme. Then the structure function becomes

$$\begin{aligned} F_{2,q}(x,Q^2) &= x\sum_i e_{q_i}^2 \int_x^1 \frac{\mathrm{d}\xi}{\xi} f_i(\xi,\mu_f^2)\,\times \\ &\quad \left\{\delta(1-\frac{x}{\xi}) + \frac{\alpha_s(\mu_r)}{2\pi}\left[P_{q\to qg}\left(\frac{x}{\xi}\right)\ln\frac{Q^2}{\mu_f^2} + \left(C_2^q - K_{qq}\right)\right]\right\} \\ &= x\sum_i e_{q_i}^2 \int_x^1 \frac{\mathrm{d}\xi}{\xi} f_i(\xi,\mu_f^2)\,\hat{F}_{2,i}(\frac{x}{\xi},Q^2,\mu_r,\mu_f)\,. \end{aligned} \tag{141}$$

Defining a convolution in x-space by $f \otimes_x g \equiv \int_x^1 \frac{\mathrm{d}\xi}{\xi} f(\xi)\, g\left(\frac{x}{\xi}\right)$, we see that the structure function is factorised in the form of a convolution,

$$F_{2,q}(x, Q^2) = x \sum_i e_{q_i}^2 \, f_i(\mu_f) \otimes_x \hat{F}_{2,i}(\mu_r, t) \quad \text{with} \quad t = \ln \frac{Q^2}{\mu_f^2} \, . \tag{142}$$

The long-distance physics is factored into the PDFs which depend on the *factorisation scale* μ_f. The short-distance physics is factored into the hard scattering cross section which depends on both the factorisation and the renormalisation scales. Both scales are arbitrary, unphysical scales. The finite terms depend on the *factorisation scheme*. They are not unique, as finite terms can be shifted between the short- and long-distance parts.

5.4 Parton evolution and the DGLAP equations

With Eq. (142) we again have an equation where an unphysical scale appears on the right-hand side, while the left-hand side is a physical quantity and therefore should not depend on the scale μ_f (when calculated to all orders in perturbation theory). This gives us something akin to a renormalisation group equation, which means that we can calculate how the PDFs evolve as the scale μ_f is changed. As the convolution in Eq. (142) is somewhat inconvenient, we go to Mellin space, where the convolution in the factorisation formula Eq. (142) turns into simple products. The Mellin transform is defined by

$$f(N) \equiv \int_0^1 \mathrm{d}x \, x^{N-1} f(x) \, .$$

The structure function in Mellin space then becomes

$$F_{2,q}(N, Q^2) = x \sum_i e_{q_i}^2 \, f_i(N, \mu_f^2) \, \hat{F}_{2,i}(N, \mu_r, t) \, . \tag{143}$$

As a measurable quantity, the structure function must be independent of μ_f, therefore

$$\frac{\mathrm{d}F_{2,q}(N, Q^2)}{\mathrm{d}\mu_f} = 0 \, . \tag{144}$$

Note that if F_2 is calculated to order α_s^n, we have $\mu_f^2 \, \mathrm{d}F_{2,q}(N, Q^2)/\mathrm{d}\mu_f^2 = \mathcal{O}(\alpha_s^{n+1})$. Therefore, as in the case of the renormalisation scale μ_r, the truncation of the perturbative series introduces a dependence on the unphysical scale in the observable, which gets weaker the more orders we calculate.

For simplicity, let us leave out the sum over i in Eq. (143) and consider only one quark flavour q. We obtain from Eq. (144)

$$\hat{F}_{2,q}(N, t) \frac{\mathrm{d}f_q(N, \mu_f^2)}{\mathrm{d}\mu_f^2} + f_q(N, \mu_f^2) \frac{\mathrm{d}\hat{F}_{2,q}(N, t)}{\mathrm{d}\mu_f^2} = 0 \, . \tag{145}$$

Dividing by $f_q\,\hat{F}_{2,q}$ and multiplying by μ_f^2 we obtain

$$\mu_f^2 \frac{\mathrm{d}\ln f_q(N,\mu_f^2)}{\mathrm{d}\mu_f^2} = -\mu_f^2 \frac{\mathrm{d}\ln \hat{F}_{2,q}(N,t)}{\mathrm{d}\mu_f^2} \equiv \gamma_{qq}(N)\;. \tag{146}$$

Using $t = \ln\left(Q^2/\mu_f^2\right)$ this can be written as

$$\frac{\mathrm{d}f_q(N,t)}{\mathrm{d}t} = \gamma_{qq}(N)\, f_q(N,t)\;, \tag{147}$$

where

$$\gamma_{qq}(N) = \int_0^1 \mathrm{d}x\, x^{N-1} P_{qq}(x) = P_{qq}(N)\;. \tag{148}$$

$\gamma_{qq}(N)$ is called the *anomalous dimension* because it measures the deviation of $\hat{F}_{2,q}$ from its naïve scaling dimension. It corresponds to the Mellin transform of the splitting functions.

Very importantly, Eq. (147) implies that the *scale dependence* of the parton densities can be calculated in perturbation theory. The PDFs themselves are non-perturbative, so they have to be extracted from experiment. However, the universality of the PDFs (for each flavour) and the calculable scale dependence means that we can measure the PDFs in one process at a certain scale and then use them in another process at a different scale.

A rigorous treatment based on operator product expansion and the renormalisation group equations extends the above result to all orders in perturbation theory, leading to

$$\boxed{\frac{\partial}{\partial t} f_{q_i}(x,t) = \int_x^1 \frac{\mathrm{d}\xi}{\xi} P_{q_i/q_j}\left(\frac{x}{\xi}, \alpha_s(t)\right) f_{q_j}(\xi,t)\;.} \tag{149}$$

The splitting functions P_{q_i/q_j} can be calculated as a power series in α_s:

$$P_{q_i/q_j}(x,\alpha_s) = \frac{\alpha_s}{2\pi} P_{ij}^{(0)}(x) + \left(\frac{\alpha_s}{2\pi}\right)^2 P_{ij}^{(1)}(x) + \left(\frac{\alpha_s}{2\pi}\right)^3 P_{ij}^{(2)}(x) + \mathcal{O}(\alpha_s^4)\,. \tag{150}$$

Equation (149) holds for distributions which are *non-singlets* under the flavour group: either a single flavour or a combination $q_{\mathrm{ns}} = f_{q_i} - f_{q_j}$ with q_i, q_j being a quark or antiquark of any flavour. More generally, the evolution equation is a $(2n_f+1)$-dimensional matrix equation in the space of quarks, antiquarks and gluons,

$$\frac{\partial}{\partial t}\begin{pmatrix} f_{q_i}(x,t) \\ f_g(x,t) \end{pmatrix} = \sum_{q_j,\bar{q}_j} \int_x^1 \frac{d\xi}{\xi} \begin{pmatrix} P_{q_i/q_j}(\frac{x}{\xi},\alpha_s(t)) & P_{q_i/g}(\frac{x}{\xi},\alpha_s(t)) \\ P_{g/q_j}(\frac{x}{\xi},\alpha_s(t)) & P_{g/g}(\frac{x}{\xi},\alpha_s(t)) \end{pmatrix} \begin{pmatrix} f_{q_j}(\xi,t) \\ f_g(\xi,t) \end{pmatrix}\;. \tag{151}$$

Equation (151) and (149) are called *DGLAP equations*, named after Dokshitzer [32], Gribov, Lipatov [46] and Altarelli, Parisi [3]. They are among the most important equations in perturbative QCD.

Note that, because of charge conjugation invariance and $SU(N_F)$ flavour symmetry, the splitting functions $P_{q/g}$ and $P_{g/q}$ are independent of the quark flavour and the same for quarks and antiquarks.

Defining the singlet distribution

$$\Sigma(x,t) = \sum_{i=1}^{N_F} [\, f_{q_i}(x,t) + f_{\bar{q}_i}(x,t) \,] \tag{152}$$

and taking into account the considerations above, Eq. (151) simplifies to

$$\frac{\partial}{\partial t} \begin{pmatrix} \Sigma(x,t) \\ g(x,t) \end{pmatrix} = \int_x^1 \frac{d\xi}{\xi} \begin{pmatrix} P_{q/q}(\frac{x}{\xi}, \alpha_s(t)) & 2N_F\, P_{q/g}(\frac{x}{\xi}, \alpha_s(t)) \\ P_{g/q}(\frac{x}{\xi}, \alpha_s(t)) & P_{g/g}(\frac{x}{\xi}, \alpha_s(t)) \end{pmatrix} \begin{pmatrix} \Sigma(\xi,t) \\ g(\xi,t) \end{pmatrix} . \tag{153}$$

The leading-order splitting functions including the regulating contributions at $x = 1$ are given by

$$\begin{aligned} P^{(0)}_{q/q}(x) &= C_F \Big\{ \frac{1+x^2}{(1-x)_+} + \frac{3}{2}\,\delta(1-x) \Big\} \\ P^{(0)}_{q/g}(x) &= T_R \Big\{ x^2 + (1-x)^2 \Big\} \quad T_R = \frac{1}{2} \\ P^{(0)}_{g/q}(x) &= C_F \Big\{ \frac{1+(1-x)^2}{x} \Big\} \\ P^{(0)}_{g/g}(x) &= 2N_c \Big\{ \frac{x}{(1-x)_+} + \frac{1-x}{x} + x(1-x) \Big\} \\ &\quad + \delta(1-x)[\frac{11}{6} N_c - \frac{2}{3} N_F T_R] \,, \end{aligned} \tag{154}$$

where the so-called *plus prescription* is used in Eq. (154), defined by

$$\int_0^1 dx f(x) \left(\frac{1}{1-x} \right)_+ = \int_0^1 dx\, \frac{f(x) - f(1)}{1-x}$$

6 Outlook

Perturbative QCD is a fascinating field with many facets. On the phenomenological side, the impressive experimental tests of the Standard Model achieved to date would have been impossible without the progress in calculating higher-order QCD corrections in the last few decades. Furthermore, important insights have been gained about the infrared structure of QCD at higher orders, the limitations of perturbation theory and the mathematical structure of scattering amplitudes. Equipped with this knowledge, we are well prepared to face the next challenges in collider physics.

Acknowledgements

I would like to thank the organisers of the European Schools of High Energy Physics 2023 for giving me the opportunity to give these lectures and for the excellent organisation. I also would like to thank the discussion leaders for their engagement and the students for their active participation and interesting questions.

References

[1] https://feynrules.irmp.ucl.ac.be/.

[2] A. Accardi et al. Electron Ion Collider: The Next QCD Frontier: Understanding the glue that binds us all. *Eur. Phys. J. A*, 52(9):268, 2016.

[3] Guido Altarelli and G. Parisi. Asymptotic Freedom in Parton Language. *Nucl. Phys.*, B126:298–318, 1977.

[4] Charalampos Anastasiou, Claude Duhr, Falko Dulat, Franz Herzog, and Bernhard Mistlberger. Higgs Boson Gluon-Fusion Production in QCD at Three Loops. *Phys. Rev. Lett.*, 114:212001, 2015.

[5] P. A. Baikov, K. G. Chetyrkin, and J. H. Kühn. Quark Mass and Field Anomalous Dimensions to $\mathcal{O}(\alpha_s^5)$. *JHEP*, 10:076, 2014.

[6] P. A. Baikov, K. G. Chetyrkin, and J. H. Kühn. Five-loop fermion anomalous dimension for a general gauge group from four-loop massless propagators. *JHEP*, 04:119, 2017.

[7] P. A. Baikov, K. G. Chetyrkin, and J. H. Kühn. Five-Loop Running of the QCD coupling constant. *Phys. Rev. Lett.*, 118(8):082002, 2017.

[8] Matteo Becchetti, Roberto Bonciani, Vittorio Del Duca, Valentin Hirschi, Francesco Moriello, and Armin Schweitzer. Next-to-leading order corrections to light-quark mixed QCD-EW contributions to Higgs boson production. *Phys. Rev. D*, 103(5):054037, 2021.

[9] Zvi Bern and David A. Kosower. Color decomposition of one loop amplitudes in gauge theories. *Nucl. Phys. B*, 362:389–448, 1991.

[10] S. Bethke, Z. Kunszt, D. E. Soper, and W. James Stirling. New jet cluster algorithms: Next-to-leading order QCD and hadronization corrections. *Nucl. Phys.*, B370:310–334, 1992. [Erratum: Nucl. Phys.B523,681(1998)].

[11] Georgios Billis, Bahman Dehnadi, Markus A. Ebert, Johannes K. L. Michel, and Frank J. Tackmann. Higgs pT Spectrum and Total Cross Section with Fiducial Cuts at Third Resummed and Fixed Order in QCD. *Phys. Rev. Lett.*, 127(7):072001, 2021.

[12] C. G. Bollini and J. J. Giambiagi. Dimensional Renormalization: The Number of Dimensions as a Regularizing Parameter. *Nuovo Cim.*, B12:20–26, 1972.

[13] Marco Bonetti, Erik Panzer, and Lorenzo Tancredi. Two-loop mixed QCD-EW corrections to $q\bar{q} \to Hg, qg \to Hq$, and $\bar{q}g \to H\bar{q}$. *JHEP*, 06:115, 2022.

[14] Matteo Cacciari, Gavin P. Salam, and Gregory Soyez. The Anti-k(t) jet clustering algorithm. *JHEP*, 04:063, 2008.

[15] John Campbell and Tobias Neumann. Third order QCD predictions for fiducial W-boson production. *JHEP*, 11:127, 2023.

[16] S. Catani and M. H. Seymour. A General algorithm for calculating jet cross-sections in NLO QCD. *Nucl. Phys.*, B485:291–419, 1997. [Erratum: Nucl. Phys.B510,503(1998)].

[17] S. Catani, L. Trentadue, G. Turnock, and B.R. Webber. Resummation of large logarithms in e+ e- event shape distributions. *Nucl. Phys. B*, 407:3–42, 1993.

[18] Stefano Catani, Simone Devoto, Massimiliano Grazzini, Stefan Kallweit, and Javier Mazzitelli.

Top-quark pair hadroproduction at NNLO: differential predictions with the $\overline{MS}$ mass. *JHEP*, 08(08):027, 2020.

[19] Stefano Catani and Massimiliano Grazzini. The soft gluon current at one loop order. *Nucl. Phys.*, B591:435–454, 2000.

[20] X. Chen, T. Gehrmann, E. W. N. Glover, A. Huss, and J. Mo. NNLO QCD corrections in full colour for jet production observables at the LHC. *JHEP*, 09:025, 2022.

[21] Xuan Chen, Thomas Gehrmann, Nigel Glover, Alexander Huss, Tong-Zhi Yang, and Hua Xing Zhu. Transverse mass distribution and charge asymmetry in W boson production to third order in QCD. *Phys. Lett. B*, 840:137876, 2023.

[22] K. G. Chetyrkin, G. Falcioni, F. Herzog, and J. A. M. Vermaseren. Five-loop renormalisation of QCD in covariant gauges. *JHEP*, 10:179, 2017. [Addendum: JHEP12,006(2017)].

[23] K. G. Chetyrkin and M. Steinhauser. The Relation between the MS-bar and the on-shell quark mass at order alpha(s)**3. *Nucl. Phys. B*, 573:617–651, 2000.

[24] M. Czakon, R. V. Harlander, J. Klappert, and M. Niggetiedt. Exact Top-Quark Mass Dependence in Hadronic Higgs Production. *Phys. Rev. Lett.*, 127(16):162002, 2021. [Erratum: Phys.Rev.Lett. 131, 179901 (2023)].

[25] Michał Czakon, Felix Eschment, Marco Niggetiedt, Rene Poncelet, and Tom Schellenberger. Top-Bottom Interference Contribution to Fully-Inclusive Higgs Production. 12 2023.

[26] Luc Darmé et al. UFO 2.0: the 'Universal Feynman Output' format. *Eur. Phys. J. C*, 83(7):631, 2023.

[27] G. Das, S. Moch, and A. Vogt. Approximate four-loop QCD corrections to the Higgs-boson production cross section. *Phys. Lett. B*, 807:135546, 2020.

[28] Joshua Davies, Matthias Steinhauser, and David Wellmann. Completing the hadronic Higgs boson decay at order α_s^4. *Nucl. Phys.*, B920:20–31, 2017.

[29] Vittorio Del Duca, Lance J. Dixon, and Fabio Maltoni. New color decompositions for gauge amplitudes at tree and loop level. *Nucl. Phys. B*, 571:51–70, 2000.

[30] G. Dissertori, I. G. Knowles, and M. Schmelling. *Quantum Chromodynamics: High energy experiments and theory*. International Series of Monographs on Physics No. 115, Oxford University Press, 2005.

[31] Lance J. Dixon. A brief introduction to modern amplitude methods. In *Theoretical Advanced Study Institute in Elementary Particle Physics: Particle Physics: The Higgs Boson and Beyond*, pages 31–67, 2014.

[32] Yuri L. Dokshitzer. Calculation of the Structure Functions for Deep Inelastic Scattering and e+ e- Annihilation by Perturbation Theory in Quantum Chromodynamics. *Sov. Phys. JETP*, 46:641–653, 1977. [Zh. Eksp. Teor. Fiz.73,1216(1977)].

[33] Yuri L. Dokshitzer, G. D. Leder, S. Moretti, and B. R. Webber. Better jet clustering algorithms. *JHEP*, 08:001, 1997.

[34] Claude Duhr, Falko Dulat, and Bernhard Mistlberger. Charged current Drell-Yan production at N^3LO. *JHEP*, 11:143, 2020.

[35] Falko Dulat, Achilleas Lazopoulos, and Bernhard Mistlberger. iHixs 2 — Inclusive Higgs cross sections. *Comput. Phys. Commun.*, 233:243–260, 2018.

[36] Matteo Fael, Fabian Lange, Kay Schönwald, and Matthias Steinhauser. A semi-analytic method to compute Feynman integrals applied to four-loop corrections to the $\overline{\rm MS}$-pole quark mass relation. *JHEP*, 09:152, 2021.

[37] J. Fleischer, F. Jegerlehner, O. V. Tarasov, and O. L. Veretin. Two loop QCD corrections of the massive fermion propagator. *Nucl. Phys. B*, 539:671–690, 1999. [Erratum: Nucl.Phys.B 571, 511–512 (2000)].

[38] H. Fritzsch, Murray Gell-Mann, and H. Leutwyler. Advantages of the Color Octet Gluon Picture. *Phys. Lett.*, 47B:365–368, 1973.

[39] Einan Gardi and Georges Grunberg. Power corrections in the single dressed gluon approximation: The Average thrust as a case study. *JHEP*, 11:016, 1999.

[40] A. Gehrmann-De Ridder, T. Gehrmann, E. W. N. Glover, and G. Heinrich. NNLO corrections to event shapes in e+ e- annihilation. *JHEP*, 12:094, 2007.

[41] A. Gehrmann-De Ridder, T. Gehrmann, E. W. N. Glover, and G. Heinrich. Jet rates in electron-positron annihilation at O(alpha(s)**3) in QCD. *Phys. Rev. Lett.*, 100:172001, 2008.

[42] A. Gehrmann-De Ridder, T. Gehrmann, E. W. N. Glover, A. Huss, and J. Pires. Triple Differential Dijet Cross Section at the LHC. *Phys. Rev. Lett.*, 123(10):102001, 2019.

[43] Murray Gell-Mann. A Schematic Model of Baryons and Mesons. *Phys. Lett.*, 8:214–215, 1964.

[44] N. Gray, David J. Broadhurst, W. Grafe, and K. Schilcher. Three Loop Relation of Quark (Modified) Ms and Pole Masses. *Z. Phys. C*, 48:673–680, 1990.

[45] Massimiliano Grazzini, S. Kallweit, Jonas M. Lindert, Stefano Pozzorini, and Marius Wiesemann. NNLO QCD + NLO EW with Matrix+OpenLoops: precise predictions for vector-boson pair production. *JHEP*, 02:087, 2020.

[46] V. N. Gribov and L. N. Lipatov. Deep inelastic e p scattering in perturbation theory. *Sov. J. Nucl. Phys.*, 15:438–450, 1972. [Yad. Fiz.15,781(1972)].

[47] David J. Gross and Frank Wilczek. Ultraviolet Behavior of Nonabelian Gauge Theories. *Phys. Rev. Lett.*, 30:1343–1346, 1973. [,271(1973)].

[48] Franz Gross et al. 50 Years of Quantum Chromodynamics. *Eur. Phys. J. C*, 83:1125, 2023.

[49] Andrey G. Grozin, Peter Marquard, Alexander V. Smirnov, Vladimir A. Smirnov, and Matthias Steinhauser. Matching the heavy-quark fields in QCD and HQET at four loops. *Phys. Rev. D*, 102(5):054008, 2020.

[50] Robert V. Harlander and Matthias Steinhauser. rhad: A Program for the evaluation of the hadronic R ratio in the perturbative regime of QCD. *Comput. Phys. Commun.*, 153:244–274, 2003.

[51] A. Heister et al. Studies of QCD at e+ e- centre-of-mass energies between 91-GeV and 209-GeV. *Eur. Phys. J. C*, 35:457–486, 2004.

[52] F. Herzog, B. Ruijl, T. Ueda, J. A. M. Vermaseren, and A. Vogt. The five-loop beta function of Yang-Mills theory with fermions. *JHEP*, 02:090, 2017.

[53] Gregor Kälin. Cyclic Mario worlds — color-decomposition for one-loop QCD. *JHEP*, 04:141,

2018.

[54] Vardan Khachatryan et al. Measurement and QCD analysis of double-differential inclusive jet cross sections in pp collisions at $\sqrt{s} = 8$ TeV and cross section ratios to 2.76 and 7 TeV. *JHEP*, 03:156, 2017.

[55] T. Kinoshita. Mass singularities of Feynman amplitudes. *J. Math. Phys.*, 3:650–677, 1962.

[56] Stefan Kluth. Tests of Quantum Chromo Dynamics at e+ e- Colliders. *Rept. Prog. Phys.*, 69:1771–1846, 2006.

[57] E. Laenen. QCD. In *Proceedings, 2014 European School of High-Energy Physics (ESHEP 2014): Garderen, The Netherlands, June 18 - July 01 2014*, pages 1–58, 2016.

[58] T. D. Lee and M. Nauenberg. Degenerate Systems and Mass Singularities. *Phys. Rev.*, 133:B1549–B1562, 1964. [,25(1964)].

[59] K. Long. QCD at high-energy (experiments). 2002. [Nucl. Phys. Proc. Suppl.117,242(2003)].

[60] Thomas Luthe, Andreas Maier, Peter Marquard, and York Schröder. Five-loop quark mass and field anomalous dimensions for a general gauge group. *JHEP*, 01:081, 2017.

[61] Thomas Luthe, Andreas Maier, Peter Marquard, and York Schröder. The five-loop Beta function for a general gauge group and anomalous dimensions beyond Feynman gauge. *JHEP*, 10:166, 2017.

[62] F. Maltoni, K. Paul, T. Stelzer, and S. Willenbrock. Color Flow Decomposition of QCD Amplitudes. *Phys. Rev. D*, 67:014026, 2003.

[63] Peter Marquard, Alexander V. Smirnov, Vladimir A. Smirnov, Matthias Steinhauser, and David Wellmann. $\overline{\rm MS}$-on-shell quark mass relation up to four loops in QCD and a general SU(N) gauge group. *Phys. Rev. D*, 94(7):074025, 2016.

[64] Simone Marzani, Gregory Soyez, and Michael Spannowsky. *Looking inside jets: an introduction to jet substructure and boosted-object phenomenology*, volume 958. Springer, 2019.

[65] Tom Melia. Proof of a new colour decomposition for QCD amplitudes. *JHEP*, 12:107, 2015.

[66] Kirill Melnikov and Timo van Ritbergen. The Three loop relation between the MS-bar and the pole quark masses. *Phys. Lett. B*, 482:99–108, 2000.

[67] Bernhard Mistlberger. Higgs boson production at hadron colliders at $\mathrm{N^3LO}$ in QCD. *JHEP*, 05:028, 2018.

[68] Alexander Ochirov and Ben Page. Full Colour for Loop Amplitudes in Yang-Mills Theory. *JHEP*, 02:100, 2017.

[69] H. David Politzer. Reliable Perturbative Results for Strong Interactions? *Phys. Rev. Lett.*, 30:1346–1349, 1973. [,274(1973)].

[70] Ted C. Rogers. An overview of transverse-momentum–dependent factorization and evolution. *Eur. Phys. J. A*, 52(6):153, 2016.

[71] Gavin P. Salam. Towards Jetography. *Eur. Phys. J. C*, 67:637–686, 2010.

[72] Peter Skands. Introduction to QCD. In *Theoretical Advanced Study Institute in Elementary Particle Physics: Searching for New Physics at Small and Large Scales*, pages 63–124, 2017.

[73] George F. Sterman and Steven Weinberg. Jets from Quantum Chromodynamics. *Phys. Rev. Lett.*, 39:1436, 1977.

[74] Gerard 't Hooft and M. J. G. Veltman. Regularization and Renormalization of Gauge Fields. *Nucl. Phys.*, B44:189–213, 1972.

[75] Z. Trocsanyi. QCD for collider experiments. In *Proceedings, 2013 European School of High-Energy Physics (ESHEP 2013): Paradfurdo, Hungary, June 5-18, 2013*, pages 65–116, 2015.

[76] T. van Ritbergen, J. A. M. Vermaseren, and S. A. Larin. The Four loop beta function in quantum chromodynamics. *Phys. Lett.*, B400:379–384, 1997.

[77] R. L. Workman et al. Review of Particle Physics. *PTEP*, 2022:083C01, 2022.

[78] G Zweig. An SU_3 model for strong interaction symmetry and its breaking; Version 1. Technical Report CERN-TH-401, CERN, Geneva, Jan 1964.